ORIGINAL RESEARCH

Arginase II Contributes to the Ca^{2+}/CaMKII/eNOS Axis by Regulating Ca^{2+} Concentration Between the Cytosol and Mitochondria in a p32-Dependent Manner

Bon-Hyeock Koo, MA;* Hye-Mi Hwang, MA;* Bong-Gu Yi, MA; Hyun Kyo Lim, MD; Byeong Hwa Jeon, MD; Kwang Lae Hoe, PhD; Young-Guen Kwon, PhD; Moo-Ho Won, PhD; Young Myeong Kim, PhD; Dan E. Berkowitz, MD; Sungwoo Ryoo, PhD

***Background*—**Arginase II activity contributes to reciprocal regulation of endothelial nitric oxide synthase (eNOS). We tested the hypotheses that arginase II activity participates in the regulation of Ca^{2+}/Ca^{2+}/calmodulin-dependent kinase II/eNOS activation, and this process is dependent on mitochondrial p32.

***Methods and Results*—**Downregulation of arginase II increased the concentration of cytosolic Ca^{2+} ($[Ca^{2+}]c$) and decreased mitochondrial Ca^{2+} ($[Ca^{2+}]m$) in microscopic and fluorescence-activated cell sorting analyses, resulting in augmented eNOS Ser1177 phosphorylation and decreased eNOS Thr495 phosphorylation through Ca^{2+}/Ca^{2+}/calmodulin-dependent kinase II. These changes were observed in human umbilical vein endothelial cells treated with small interfering RNA against p32 (sip32). Using matrix-assisted laser desorption/ionization time-of-flight mass spectrometry, fluorescence immunoassay, and ion chromatography, inhibition of arginase II reduced the amount of spermine, a binding molecule, and the release of Ca^{2+} from p32. In addition, arginase II gene knockdown using small interfering RNA and knockout arginase II-null mice resulted in reduced p32 protein level. In the aortas of wild-type mice, small interfering RNA against p32 induced eNOS Ser1177 phosphorylation and enhanced NO-dependent vasorelaxation. Arginase activity, p32 protein expression, spermine amount, and $[Ca^{2+}]m$ were increased in the aortas from apolipoprotein E ($ApoE^{-/-}$) mice fed a high-cholesterol diet, and intravenous administration of small interfering RNA against p32 restored Ca^{2+}/Ca^{2+}/calmodulin-dependent kinase II-dependent eNOS Ser1177 phosphorylation and improved endothelial dysfunction. The effects of arginase II downregulation were not associated with elevated NO production when tested in aortic endothelia from eNOS knockout mice.

***Conclusions*—**These data demonstrate a novel function of arginase II in regulation of Ca^{2+}-dependent eNOS phosphorylation. This novel mechanism drives arginase activation, mitochondrial dysfunction, endothelial dysfunction, and atherogenesis. **(*J Am Heart Assoc*. 2018;7:e009579. DOI: 10.1161/JAHA.118.009579.)**

Key Words: Arginase II • atherogenesis • Calcium signaling • eNOS • p32

Nitric oxide (NO) plays a key role in the maintenance of vascular homeostasis by modulating vascular tone, as well as vascular smooth muscle cell proliferation and migration. Endothelial dysfunction defined as decreased NO production is considered an initial and critical event in vascular diseases such as atherogenesis, causing vascular stiffness.[1] In reciprocal regulation of NO synthase (NOS) by arginase, upregulation of arginase activity contributes to vasoregulatory dysfunction.[2]

Two isoforms of arginase, arginase I, and arginase II encoded by different genes,[3] exhibited distinct expression patterns.[4] Arginase I is considered the hepatic isoform

From the Department of Biology, School of Medicine (B.H.K., H.M.H., B.G.Y., S.R.), Department of Neurobiology, School of Medicine (M.H.W.), and College of Natural Sciences and Departments of Molecular and Cellular Biochemistry, School of Medicine (Y.M.K.), Kangwon National University, Chuncheon, Korea; Department of Anesthesiology and Pain Medicine, Yonsei University Wonju College of Medicine, Wonju, Korea (H.K.L.); Infectious Signaling Network Research Center, Department of Physiology, School of Medicine (B.H.J.), Department of New Drug Discovery and Development (K.L.H.), Chungnam National University, Daejeon, Korea; Department of Biochemistry, Yonsei University, Seoul, Korea (Y.G.K.); Department of Anesthesiology and Critical Care Medicine, Johns Hopkins University, Baltimore, MD (D.E.B.).

Accompanying Figures S1 through S10 are available at https://www.ahajournals.org/doi/suppl/10.1161/JAHA.118.009579

*Dr Koo and Hwang contributed equally to this work.

Correspondence to: Sungwoo Ryoo, PhD, Department of Biology, Kangwon National University, Kangwondae-gil 1, Chuncheon, Kangwon-do, 24341. E-mail: ryoosw08@kangwon.ac.kr

Received April 23, 2018; accepted July 26, 2018.

Clinical Perspective

What Is New?

- Arginase II inhibition decreased [Ca^{2+}]m and increased [Ca^{2+}]c, resulting in Ca^{2+}/Ca^{2+}/calmodulin-dependent kinase II-dependent eNOS activation.
- The regulation of intracellular [Ca^{2+}] by arginase II is p32-dependent.
- p32 knockdown with small interfering RNA enhanced the Ca^{2+}/Ca^{2+}/Ca^{2+}/calmodulin-dependent kinase II/eNOS activation axis and improved endothelial dysfunction in apolipoprotein E ($ApoE^{-/-}$) mice fed a high-cholesterol diet.
- Arginase II participates in endothelial dysfunction by contributing to the regulation of intracellular Ca^{2+} concentration in an NO-independent manner.

What Are the Clinical Implications?

- p32, an a cytosol/mitochondria Ca^{2+} regulator, was identified as a new therapeutic target for vascular disorders in which NO production was interrupted and injurious reactive oxygen species generation was promoted.

catalyzing the final step in the urea cycle, and its expression can be induced by hypoxia and lipopolysaccharide.[5] Arginase II, as the extrahepatic isoform, is the principal form in human and mouse aortic endothelial cells (ECs) and provides L-ornithine for the synthesis of polyamines, putrescine, spermidine, and spermine (SPM), associated with cell proliferation and differentiation.[6,7] Arginase II is also inducible by hypoxia, lipopolysaccharide, and tumor necrosis factor-α,[8–10] and increased arginase II activity in ECs has recently been extended to other disorders in animal models, including aging,[11] ischemic reperfusion,[12,13] hypertension,[14,15] balloon injury,[16] and atherosclerosis.[2] Although arginase II participates in the endothelial dysfunction, the mechanism through which endothelial NOS activity is regulated remains unclear. However, a novel mechanism showed that oxidized low-density lipoprotein triggered translocation of arginase II from mitochondria to the cytoplasm via mitochondrial processing peptidase with a simultaneous increase in arginase activity that drove endothelial nitric oxide synthase (eNOS) uncoupling by depleting the substrate pool available for NO biosynthesis.[17] Similarly, we also showed that an arginase inhibitor-enhanced eNOS phosphorylation at Ser1177[18] and arginase II inhibition improved the loss of mitochondrial membrane potential by a Ca^{2+}-dependent mechanism and prevented mitochondrial reactive oxygen species (ROS) production.[19]

eNOS activity can be regulated by various extracellular signals, including subcellular targeting, and protein-protein interactions. In these regulations, Ca^{2+} principally contributes to modulation of eNOS activity. Activated calmodulin (Ca^{2+}/CaM) from increased cytosolic Ca^{2+} level binds to the canonical CaM-binding domain in eNOS that promotes the alignment of the oxygenase and reductase domains of eNOS and prevents eNOS Thr495 phosphorylation by protein kinase C, leading to efficient NO synthesis. Ca^{2+}/CaM can also activate Ca^{2+}/calmodulin-dependent protein kinase II (CaMKII), which participates in the phosphorylation of eNOS Ser1177 to increase NO release.[20,21] Intracellular Ca^{2+} can be transported and stored in endoplasmic (sarcoplasmic) reticulum and mitochondria. Ca^{2+} uptake by mitochondria controls cellular Ca^{2+} homeostasis, regulates the oxidative phosphorylation rate and ATP synthesis, and attenuates transient cytosolic Ca^{2+}.[22]

p32, also known as HABP1 (hyaluronan-binding protein 1), is a receptor for gC1qR (globular head domains complement 1q), or C1qbp (complement 1q-binding protein), and has been recognized as a pre-mRNA splicing factor SF2-binding protein in the nucleus[23] and a receptor interacting with the complement component C1q on the cell surface.[24] Although p32 can be existed in multicellular compartments, it is predominantly targeted to mitochondria because of the mitochondrial targeting sequence contained in the 73N-terminal amino acids.[25] Functional studies have shown that p32 is required for the induction of mitochondria-dependent cell death[26,27] and for the metabolic shift between oxidative phosphorylation and aerobic glycolysis.[28] Moreover, the crystal structure of p32 has been determined and indicates that p32 can form a pore-like homotrimer and may serve as a high-capacity divalent cation storage protein.[29] However, in ECs, the function of p32 and its regulatory mechanism remain unknown.

Therefore, we investigated whether arginase II activity participates in the regulation of cytosolic Ca^{2+} concentration ([Ca^{2+}]c) and mitochondrial Ca^{2+} concentration ([Ca^{2+}]m) that may be associated with Ca^{2+}-dependent eNOS activation. We also examined the function of p32 as a Ca^{2+}-modulating protein in mitochondria and investigated the regulatory mechanism between arginase II and p32. Finally, we tested whether the small interfering RNA (siRNA) against p32 (sip32) restored endothelial dysfunction in the atherogenic mouse model ($ApoE^{-/-}$-null) fed a high-cholesterol diet (HCD).

Materials and Methods

The data, analytic methods, and study materials will be made available to other researchers for purposes of reproducing the results or replicating the procedure. The data that support the findings of this study are available from the corresponding author upon reasonable request.

Materials

The 2(S)-amino-6-boronohexanoic acid (ABH), NG-nitro-L-arginine methyl ester, manganese (III) tetrakis (4-benzoic acid) porphyrin chloride (MnTBAP), KN-93, and BAPTA-AM were purchased from Calbiochem (Darmstadt, Germany). All other chemicals including polyamine and L-arginine were obtained from Sigma (St. Louis, MO) unless otherwise stated. Anti-sera against eNOS, phospho-eNOS (Ser1177, Thr 495), phosphor-CaMKII, and pan-actin were obtained from BD Biosciences (San Jose, CA), and p32 and p32 antiserum was from Abcam Co. (Cambridge, MA). siRNA against arginase II (siArgII, sc-29729) and scramble RNA (scmRNA, sc-37007) were purchased from Santa Cruz Biotechnology (Dallas, TX).

Cell Culture and Animals

Human umbilical vein endothelial cells (HUVECs) were purchased from Cascade Biologics (Portland, OR) and maintained in Medium 200 containing low serum growth supplement according to the supplier's instructions. Male C57BL/6J wild type (WT, n=12) and male $ApoE^{-/-}$ mice (Daehan Biolink Co. Chungbuk, Korea, n=15) were obtained at 10 weeks of age and fed a normal diet (ND) or a high-cholesterol diet (HCD, D12108C, Research Diet Inc.) for 8 weeks, respectively. $ApoE^{-/-}$ mice fed an HCD were administered with scramble (scm) or siRNA against p32 (sip32) by intravenous injection (30 μmol/L/mouse per day, dissolved in PBS, with an injection volume of 50 μL) 5 times with 2-day intervals before experiments were performed. Two pairs of the arginase II knockout (KO) breeders with a C57BL/6 background were a generous gift from Professor Jaye P.F. Chin-Dusting for establishment of a colony at Kangwon National University Animal Services Facility and 10-week male mice (n=15) were used for all experiments. The study was approved in accordance with the *Guide for the Care and Use of Laboratory Animals* (approval no. KW-17002, Institutional Animal Care and Use Committee, Kangwon National University) and adhered to guidelines that are in compliance with the current international laws and policies (*Guide for the Care and Use of Laboratory Animals*, The National Academies Press, 8th edition, 2011).

Isolation of Mouse Endothelial Cells

Endothelial cells were isolated from the aorta of anesthetized mice of WT, Arg $II^{-/-}$, and $ApoE^{-/-}$ mice as previously described.[2] All experiments were performed with the second passage of endothelial cells.

siRNA Treatment and Knockdown of Mitochondrial p32

For siRNA transfection, HUVECs were incubated in starvation medium (DMEM plus 5% FBS and antibiotics) containing siRNA against p32 (sip32, 100 nmol/L, 5′-TGT CTC CGT CGG TGT GCA GC-Cy5- 3′), scramble siRNA (scmRNA) (100 nmol/L, 5′-GCT GCA CAC CGA CGG AGA CA-Cy5-3′) or no oligonucleotide for 24 hours without a reagent. Dissected thoracic aortas of mice were incubated for 24 hours in DMEM (2% FBS, 100 U/mL penicillin and 100 μg/mL streptomycin) containing sip32 (100 nmol/L, 5′-TGT CTC CTT CCG TGT GCA GA-Cy5-3′) and scmRNA (100 nmol/L, 5′-CAG CAC AGC CCT GGA GCA CC-Cy5-3′).

Arginase Activity Assay

Arginase activity was assessed by measuring urea content using α-isonitrosopropiophenone as previously described.[2] Briefly, supernatants of extracted cell lysates were prepared by incubation with lysis buffer (Tris-HCl 50 mmol/L, pH 7.5, EDTA 0.1 mmol/L, and protease inhibitors) for 30 minutes at 4°C and centrifugation for 20 minutes at 14 000 *g* at 4°C. Aortic vessel samples were assayed following homogenization in lysis buffer.

Measurement of NO and ROS

Aortic rings from 10-week-old male C57BL/6 WT mice were prepared for assays of fluorescent probe labeling of superoxide (dihydroethidine [DHE] 1 μmol/L, for 5 minutes with 30-seconds intervals) or NO (4-amino-5-methylamino-2′,7′-difluorofluorescein diacetate ([DAF-FM DA], 5 μmol/L, for 5 minutes with 30-seconds intervals). Images were acquired using an Olympus BX51 epifluorescence microscope. Fluorescence intensity was measured as previously described[2] using Metamorph software.

Aortic Vascular Tension Assay

Heparin was administered 1 hour before mice were euthanized. Mice were anesthetized using isoflurane, and the thoracic aorta from aortic root to the bifurcation of the iliac arteries was rapidly isolated and cut into 1.5-mm rings. The aortic rings were placed in ice-cold oxygenated Krebs-Ringer bicarbonate buffer (NaCl 118.3 mmol/L, KCl 4.7 mmol/L, MgSO4 1.2 mmol/L, CaCl2 1.6 mmol/L, NaHCO3 25 mmol/L, glucose 11.1 mmol/L; pH 7.4) and suspended between 2 wire stirrups (150 mm) in a myograph (Multi Myograph System, DMT-620) containing 10-mL Krebs-Ringer (95% O_2-5% CO_2, pH 7.4, 37°C). One stirrup was connected to a 3-dimensional micromanipulator, and the other to a force transducer. The aortic rings were passively stretched at 10-minutes intervals in increments of 100 mg to reach the optimal tone (600 mg). After the aortic rings were stretched to their optimal resting tone, the contractile response to 60 mmol/L KCl was determined. The response

to a maximal dose of KCl was used to normalize the responses to agonist across vessel rings. Dose responses to the vasoconstrictor phenylephrine (PE, 10^{-9}–10^{-5} mol/L) were assessed, and responses to the vasodilators acetylcholine (Ach, 10^{-9}–10^{-5} mol/L) and sodium nitroprusside (sodium nitroprusside, 10^{-10}–10^{-6} mol/L) were assessed after pre-constriction with PE (10^{-5} mol/L). To further confirm the NO-dependent vasorelaxation activity, aortic rings were treated with 1H-[1,2,4]oxadiazolo[4,3-a]quinoxalin-1-one (ODQ, 10^{-5} mol/L), a soluble guanylyl cyclase inhibitor.

Western Blot Analysis

Aortic vessels and cell lysates were subjected to SDS-PAGE followed by Western blot.[2] Band intensities were analyzed using NIH ImageJ.

Polyamine and L-Arginine Analyses

Intracellular concentrations of L-arginine (L-Arg) and polyamine, spermine (SPM), spermidine, and putrescine were determined using high performance liquid chromatography (HPLC) with pre-column derivatization with o-phthalaldehyde according to a modification of previously published methods.[30] Briefly, L-arginine (100 μmol/L) and polyamine (30 μmol/L/each) were added to cell lysate (0.1 mmol/L) as an internal standard. The samples were extracted on solid-phase extraction cartridges (CBA Bond elute, Varian), and the recovery rate was 87.5±3.9% to L-Arg. Eluates were dried over nitrogen and resuspended in double-distilled water for HPLC analysis. HPLC was performed on a computer-controlled Waters chromatography system (M600E) consisting of an automatic injector (M7725i, Waters Co.) and a fluorescence detector (FP-1520, Jasco Co.). Samples were incubated for 1 minute with o-phthalaldehyde reagent (5.4-mg/mL o-phthalaldehyde in borate buffer, pH 8.4, containing 0.4% 2-mercaptoethanol) before automatic injection into the HPLC. The o-phthalaldehyde derivatives of L-Arg and polyamine were separated on a 150×4.6 mm^{-5} μm Zorbax Eclipse XDB-C18 column with the fluorescence detector set at excitation 340 nm and emission 450 nm. Samples were eluted from the column with 0.96% citric acid/methanol (70:30), pH 6.8 at a flow rate of 1.5 mL/min.

$[Ca^{2+}]$m and $[Ca^{2+}]$c Measurement using Confocal Microscopy and Flow Cytometry

Direct assessment of the mitochondrial Ca^{2+} content was performed by an established loading procedure of the cells with Rhod-2 AM (ThermoFisher Scientific Co., Waltham, MA). Briefly, cells were loaded with 2.5 μmol/L Rhod-2 AM at 37°C for 1 hour in starved media. Subsequently, cells were washed free of Rhod-2 AM and incubated in Tyrode's modified solution (NaCl 150 mmol/L, KCl 4 mmol/L, $CaCl_2$ 2 mmol/L, $MgCl_2$ 2 mmol/L, HEPES 10 mmol/L and glucose 10 mmol/L). For detection of Rhod-2 AM fluorescence, a 552 nm excitation and 581-nm emission filters were used. MitoTracker green FM (ThermoFisher Scientific Co.) was incubated to confirm the mitochondria at 100 nmol/L for 1 hour and imaged at 490-nm excitation and 516-nm emission. $[Ca^{2+}]$c was monitored using Fluo-4 AM (100 nmol/L, 1 hour, ThermoFisher Scientific Co.) at 494 nm excitation, and emission at 506 nm was detected. Intensity values were normalized according to the initial fluorescence values after subtraction of background using Metamorph program (Molecular Probe).

$[Ca^{2+}]$m and $[Ca^{2+}]$c were also determined using flow cytometry (FACSCalibur). The fluorescence intensity for each sample was determined using CellQuest software. The Ca^{2+} level was determined by comparing the fold changes in the fluorescence intensities of treated cells versus control cells.

Mitochondrial Fractionation

Cells and aortic segments were homogenized twice in subcellular fractionation buffer (sucrose 250 mmol/L, HEPES 20 mmol/L, pH 7.4, KCl 10 mmol/L, $MgCl_2$ 1.5 mmol/L, EDTA 1 mmol/L, EGTA 1 mmol/L, and protease inhibitors (Roche Co.)) for 3 minutes and centrifuged at 1000 *g* for 10 minutes to remove cell debris and unbroken cells. The supernatants were centrifuged at 21 000 *g* for 45 minutes at 4°C. The cytosolic (supernatant) and mitochondrial (precipitate) fractions containing 20 μg proteins were used for subsequent Western blot analyses. Purity of the fractions was measured using Western blotting for HSP60 and actin, respectively.

MALDI-TOF Mass Spectrometry

p32 protein (200 ng in distilled water, pH7.4, Abcam Co.) and polyamine, L-Arg, and L-ornithine (10 mmol/L) were incubated for 1 hour at room temperature. MALDI-TOF mass spectrometry analyses were performed using a Bruker Autoflex speed TOF/TOF mass spectrometer (Billerica, MA). Analyses were performed in the reflector mode at a mass range of 20 000 to 45 000 m/z with an accelerating voltage of 20 kV and a delay time of 300 ns. The instrument was externally calibrated. A low-mass gate value of 20 000 m/z was selected to avoid saturation of the detector. 2,5-Dihydroxybenzoic acid at 10 mg/mL in 70% acetonitrile-0.1% trifluoroacetic acid was used as a matrix.

Fluorescence Immunoassay

Monoclonal antibody against p32 (Abcam Co. Cambridge, MA) was coated onto 96-well plates for 2 hours at 37°C with shaking at 150 rpm, and unbound antibody was removed by washing with phosphate-buffered saline with Tween 20 (PBST). Unbound sites in wells were blocked with bovine serum albumin (3% in PBST) for 1 hour at 37°C, followed by washing with PBST. The prepared p32 protein (500 ng/100 μL) was added to the wells and incubated for 2 hours at 37°C, and followed by washing with PBST. Next, different concentrations of Rhodamine B-tagged SPM were added to the wells and incubated for 1 hour at 37°C, and the wells were washed 5 times with PBST. The fluorescence intensity of each well was read at 553 nm excitation and 627 nm emission using epifluorescence microscopy (10× objective lens) equipped with the Metamorph program. K_d values were calculated using GraphPad Prism 5 software.

Ion Chromatography

p32 (10 ng and 100 ng) was added to Ca^{2+} standard solutions (1 μg/mL, Merck Co., Darmstadt, Germany) and incubated for 30 minutes at 37°C. The solutions were filtered using the centrifugal filter Amicon Ultra-4 (ultracel-3K, Cork, Ireland) and the filtrates (25 μL) were subjected to ion column (cation analytical column, 4×250 nm CS12A) chromatography (Thermo Dionex, ICS-5000+) equipped with a DC detector at a 1 mL/min flow rate.

Statistics

Each graph represents cumulative data from 3 independent experiments performed at least in triplicate. Statistical significance was determined using one-way ANOVA (mean ±SEM) with a post hoc test or t test (mean±SEM) or two-way ANOVA (mean±SD; GraphPad Prism 5 software). A $P<0.05$ was considered statistically significant.

Results

Arginase II Plays an Important Role in the Regulation of $[Ca^{2+}]m$ and $[Ca^{2+}]c$

We first analyzed the role of arginase II in the Ca^{2+} concentration changes with isolated mouse aortic ECs and HUVECs using the mitochondrial Ca^{2+}-sensitive fluorescence dye Rhod-2 AM and the cytosolic Ca^{2+}-sensitive fluorescence dye Fluo-4 AM. $[Ca^{2+}]m$ was reduced in mouse aortic ECs of arginase II KO mice compared with wild-type (WT, Figure 1A). The Rhod-2 fluorescence was clearly merged with Mito-Tracker green fluorescence. To further confirm that arginase II inhibition decreased $[Ca^{2+}]m$, HUVECs were treated with the arginase inhibitor ABH and stained with Rhod-2 AM. Consistent with the results observed in arginase II KO mice, $[Ca^{2+}]m$ was decreased (Figure 1B). Based on these data, we next determined the change in $[Ca^{2+}]c$. As shown in Figure 1C and 1D, $[Ca^{2+}]c$ was reciprocally increased in both mouse aortic ECs from arginase II KO mice and ABH-treated HUVECs. Fluorescence-activated cell sorting analysis was performed to further confirm the data. Arginase II downregulation with siRNA (siArgII) and ABH showed decreased $[Ca^{2+}]m$ (Figure 1E) and increased $[Ca^{2+}]c$ (Figure 1F). The increased $[Ca^{2+}]c$ caused by arginase inhibition was not from extracellular Ca^{2+} (Figure S1).

Increased $[Ca^{2+}]c$ Via Arginase II Downregulation Results in Phosphorylation of CaMKII and eNOS Ser1177

Since arginase inhibition increased $[Ca^{2+}]c$, CaMKII activation was investigated based on the premise that Ca^{2+}-dependent protein kinase participates in eNOS activation. In aortic lysates from arginase II KO mice, phosphorylation of CaMKII and eNOS Ser1177 was significantly increased, but eNOS Thr495 phosphorylation was reduced (Figure 2A). These results were consistent with the results observed in HUVECs treated with the arginase inhibitor ABH (Figure 2B). Next, whether phosphorylation was associated with increased $[Ca^{2+}]c$ caused by arginase inhibition was investigated using siRNA. siArgII incubation significantly blocked arginase II expression, and the phosphorylation of eNOS Ser1177 and CaMKII was enhanced without the changes in the expression levels of total protein. The phosphorylation of these proteins was completely blocked with the intracellular Ca^{2+} chelator BAPTA-AM (Figure 2C). Furthermore, CaMKII inhibition with KN93 prevented siArgII-dependent eNOS Ser1177 phosphorylation (Figure 2D). Therefore, increased $[Ca^{2+}]c$ caused by arginase downregulation augmented CaMKII-dependent eNOS Ser1177 phosphorylation and attenuated eNOS Thr495 phosphorylation.

sip32 Decreases $[Ca^{2+}]m$, Increased $[Ca^{2+}]c$, and Induces CaMKII-Dependent eNOS Ser1177 Phosphorylation

Because arginase II inhibition decreased $[Ca^{2+}]m$, the proteins participating in arginase activity-dependent regulation of $[Ca^{2+}]m$ were investigated. Among the mitochondrial proteins, we focused on a protein p32, even though its biological function associated with Ca^{2+} in mitochondria has not been clearly demonstrated. In a previous crystal structure study, p32 was shown to have structural similarity to Ca^{2+} storage protein and may serve as a high-capacity divalent cation

storage protein.[29] We designed siRNA against mitochondria-targeted p32 (sip32) and tested the efficacy according to incubation time and dose. As shown in Figure 3A (top and bottom), incubation of 100 nmol/L sip32 for 24 hours showed significant inhibition of p32 expression in both mitochondrial and cytosolic fractions. Under the same conditions, sip32 treatment decreased $[Ca^{2+}]m$ (Figure 3B) and increased $[Ca^{2+}]c$ (Figure 3C). Furthermore, sip32 dose-dependently increased the phosphorylation of CaMKII and eNOS Ser1177, however, the eNOS Thr495 phosphorylation was decreased (Figure 3D). sip32 incubation resulted in increased $[Ca^{2+}]c$ (Figure 3E) based on fluorescence-activated cell sorting analysis, and pretreatment with the CaMKII inhibitor, KN-93 prevented sip32-dependent eNOS Ser1177 phosphorylation (Figure 3F).

SPM Triggers Ca^{2+} Movement into Mitochondria in a p32-Dependent Manner

Since downregulation of arginase and p32 increased $[Ca^{2+}]c$ and reciprocally decreased $[Ca^{2+}]m$, we investigated the molecules involved in the regulation of $[Ca^{2+}]$. Therefore, $[Ca^{2+}]m$ and $[Ca^{2+}]c$ were measured after incubation with the arginase substrate, L-Arginine (L-Arg) and products L-ornithine, putrescine, spermidine, and SPM. L-Arg induced increased $[Ca^{2+}]c$, and SPM incubation decreased $[Ca^{2+}]c$ (Figure 4A). Conversely, only SPM incubation caused an increase in $[Ca^{2+}]m$ (Figure 4B). Based on these results, whether SPM acts as an activator of mitochondrial p32 was investigated by measuring the $[Ca^{2+}]m$ in sip32-treated HUVECs. sip32 prevented SPM-stimulated increase in $[Ca^{2+}]m$ based on microscopic images (Figure 4C) and fluorescence-activated cell sorting analysis (Figure S2A). Additionally, the direct interaction of SPM with p32 at a ratio of 1:1 was confirmed using MALDI-TOF analysis (Figure S2B). The SPM-induced increase in $[Ca^{2+}]m$ was dependent on intracellular Ca^{2+}, not extracelluar Ca^{2+} (Figure S2D and S2E). To further confirm the Ca^{2+}-binding capacity of p32, ion chromatography was performed (Figure S2F, Methods section). $[Ca^{2+}]$ in the filtrate was significantly reduced dose-dependently in p32 and was completely recovered with SPM preincubation (Figure S2G). These results suggest that the Ca^{2+}-storage capacity of p32 may be regulated by SPM level. Finally, we analyzed the phosphorylation of CaMKII and eNOS caused by SPM stimulation in the siRNA-preincubated HUVECs. SPM stimulation significantly reduced the phosphorylation of CaMKII and eNOS Ser1177, but increased eNOS Thr495 phosphorylation in both siRNA-untreated and -treated HUVECs (Figure 4D). Consistent with the results shown in Figure 3D, only sip32 incubation increased the phosphorylation of CaMKII and eNOS Ser1177 (Figure 4D).

Arginase II Regulates Intracellular SPM Concentration and Mitochondrial p32 Protein Concentration ([p32]m)

The previous results indicated that arginase inhibition/gene knockdown and p32 downregulation showed the same effect on Ca^{2+}-dependent eNOS phosphorylation, and SPM acts as an activator of p32-dependent increase in $[Ca^{2+}]m$. Next, whether arginase regulates the concentration of intracellular SPM and the expression of mitochondrial p32 was investigated. First, in intracellular SPM concentration analysis using HPLC, arginase inhibition and siArgII incubation significantly reduced SPM concentration (Figure 5A). siArgII-dependent downregulation of arginase II protein downregulated p32 at protein level (Figure 5B). p32 level was reduced in the aortas of arginase II KO mice, (Figure 5C), however, intracellular L-Arg and SPM concentrations did not differ from those of WT mice (Figure 5D). Conversely, increased arginase II protein level of in the aortas of eNOS KO mice and increased p32 level were observed (Figure S3A and S3B). Therefore, we hypothesized that arginase activity-dependent regulation of SPM concentration and arginase protein-dependent regulation of p32 protein levels are important mechanisms in arginase-dependent controls of $[Ca^{2+}]m$ and $[Ca^{2+}]c$. However, knockdown of p32 protein did not effect arginase II protein level or activity (Figure S4).

sip32 Induces CaMKII-Dependent eNOS Ser1177 Phosphorylation Associated With Enhanced NO Production and Vasorelaxation in the Aortas of WT Mice

Since sip32 increased $[Ca^{2+}]c$ and CaMKII-dependent eNOS activation in HUVECs, the effect of sip32 on NO production in the aortas of WT mice was investigated. First, we confirmed that sip32 incubation with aortic vessels without a transfection reagent downregulated [p32]m (Figure 6A) and induced the phosphorylation of CaMKII and eNOS Ser1177, but blocked eNOS Thr495 phosphorylation (Figure 6B). NO production in endothelia was significantly enhanced (Figure 6C) and ROS production was prevented (Figure 6D) in sip32-treated vessels compared with ABH-treated aortic vessels from WT mice and aortic vessels from arginase II KO mice. Furthermore, sip32 augmented Ach-dependent vasorelaxation (Figure 6E, WT versus WT+sip32, log EC_{50}=−6.94±0.12 versus −7.29±0.06 mol/L, E_{max}, 73.08±3.51 versus 96.61±2.15%, P<0.01) without difference in sodium nitroprusside responses (Figure 6F) and delayed PE-dose responses in vasoconstriction (Figure 6G, WT versus WT+sip32, log EC_{50}=−7.20±0.07 versus −7.14±0.08 mol/L, E_{max}, 100.90±2.66 versus 77.94±2.26%, P<0.01).

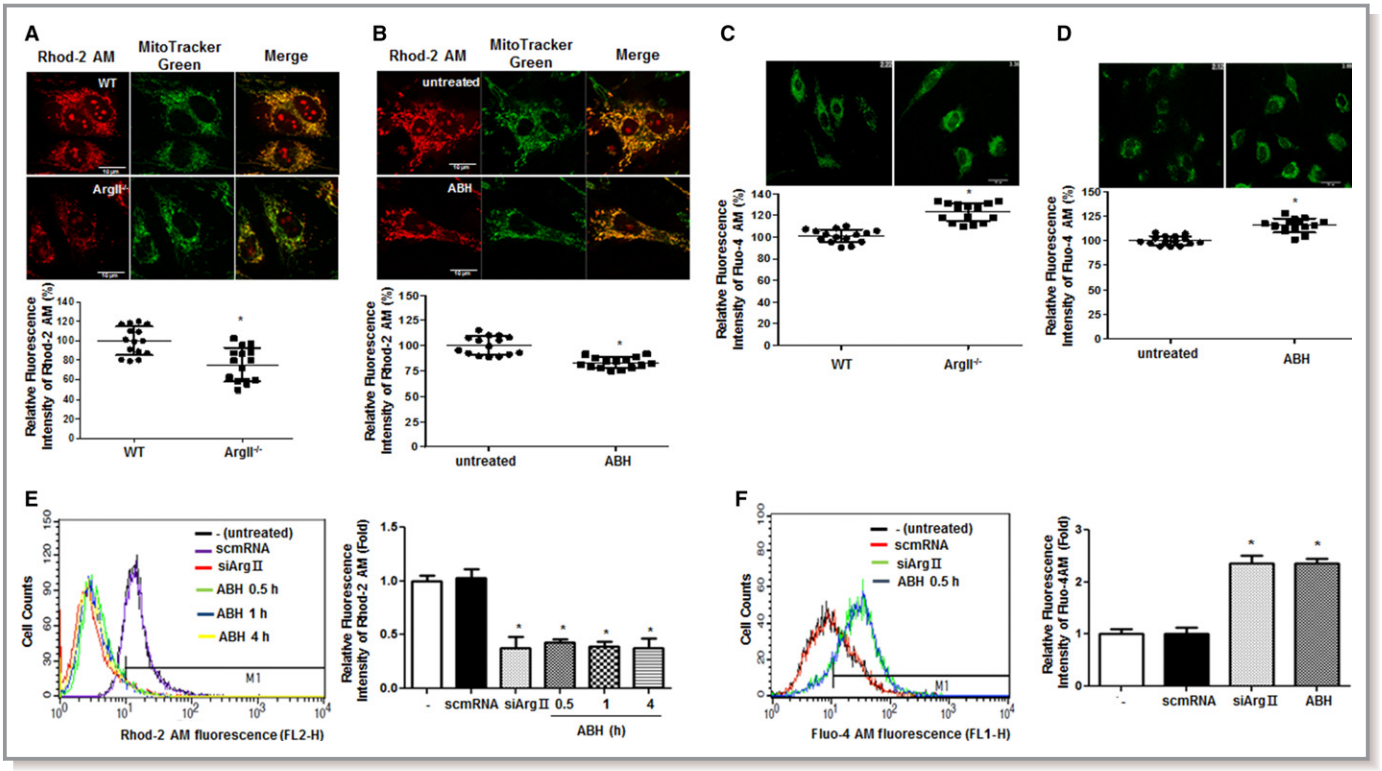

Figure 1. Arginase inhibition and arginase II gene knockout induced an increase in cytosolic Ca^{2+} level ($[Ca^{2+}]c$) and a decrease in mitochondrial Ca^{2+} level ($[Ca^{2+}]m$). A, ECs were isolated from the aortas of WT and $ArgII^{-/-}$ mice and stained with Rhod-2 AM to measure $[Ca^{2+}]m$ and MitoTracker green, a mitochondria-specific fluorescence dye. B, HUVECs were stained with Rhod-2 AM and MitoTracker green after pretreatment with the arginase inhibitor, ABH (10 μmol/L, 1 hour). Isolated mouse ECs (C) and HUVECs incubated with ABH (D) were stained with Fluo-4 AM to measure $[Ca^{2+}]c$. E, HUVECs were pretreated with siArgII, scmRNA (100 nmol/L, 24 hours), and ABH and stained with Rhod-2 AM for FACS analyses. Relative Rhod-2 AM fluorescence intensities were quantitated. F, $[Ca^{2+}]c$ in HUVECs treated with siRNAs and ABH (10 μmol/L, 4 hours) were analyzed using FACS. Relative Fluo-4 AM fluorescence intensities are presented as a bar graph. ABH indicates 2(S)-amino-6-boronohexanoic acid; $ArgII^{-/-}$, arginase II-null mice; FACS, fluorescence-activated cell sorting; EC, endothelial cells; HUVECs, human umbilical vein endothelial cells; WT, wild-type. *vs WT and untreated (-), $P<0.01$. Images are representative of 15 samples (n=4 experiments) and FACS analyses were performed 4 times.

Arginase activity, mitochondrial p32 level, SPM concentration, and $[Ca^{2+}]m$ were increased in $ApoE^{-/-}$ mice fed an HCD and intravenous administration of sip32 improved endothelial dysfunction

Next, the expression level of p32 and $[Ca^{2+}]m$ in ECs of an atherogenic animal model, ApoE-null mice fed an HCD for 8 weeks, was investigated. Arginase activity in the aortas of ApoE-null mice fed an HCD was significantly increased (Figure 7A). [p32]m level was also increased in the aortas (Figure 7B). Consistent with increased arginase activity, L-Arg concentration was decreased and SPM level was increased in the aortas of ApoE-null mice fed an HCD (Figure 7C). Conversely, arginase inhibition resulted in decreased SPM level and increased L-Arg concentration (Figure S5). Furthermore, $[Ca^{2+}]c$ was decreased and $[Ca^{2+}]m$ was increased (Figure 7D), consistent with results observed in HUVECs. Additionally, it was confirmed that HCD induces the expression of p32. [p32]m in the aortas of age-matched WT and ApoE-null mice was analyzed. As shown in Figure S6A, [p32]m was not different between these mice, however, ox-LDL time-dependently induced p32 expression (Figure S6B). Therefore, based on the results, an HCD may play an important role in p32 expression. Since sip32 enhanced NO production in mouse aortas and increased expression of p32 in the aortas from ApoE-null mice fed an HCD, we investigated whether intravenous administration of sip32 restores endothelial dysfunction in ApoE-null mice fed an HCD. Administration of sip32 downregulated increased p32 expression (Figure 7E) and improved the phosphorylation of CaMKII and eNOS Ser1177, however, eNOS Thr495 phosphorylation was decreased (Figure 7F) in the aortas of ApoE-null mice fed an HCD. Furthermore, sip32 restored the attenuated NO production (Figure 7G) and augmented ROS generation (Figure 7H) in ApoE-null mice fed an HCD. In the vascular tension assay, sip32 significantly improved Ach-dependent vasorelaxation (Figure 7I, log EC_{50}; WT versus $ApoE^{-/-}$+HCD,

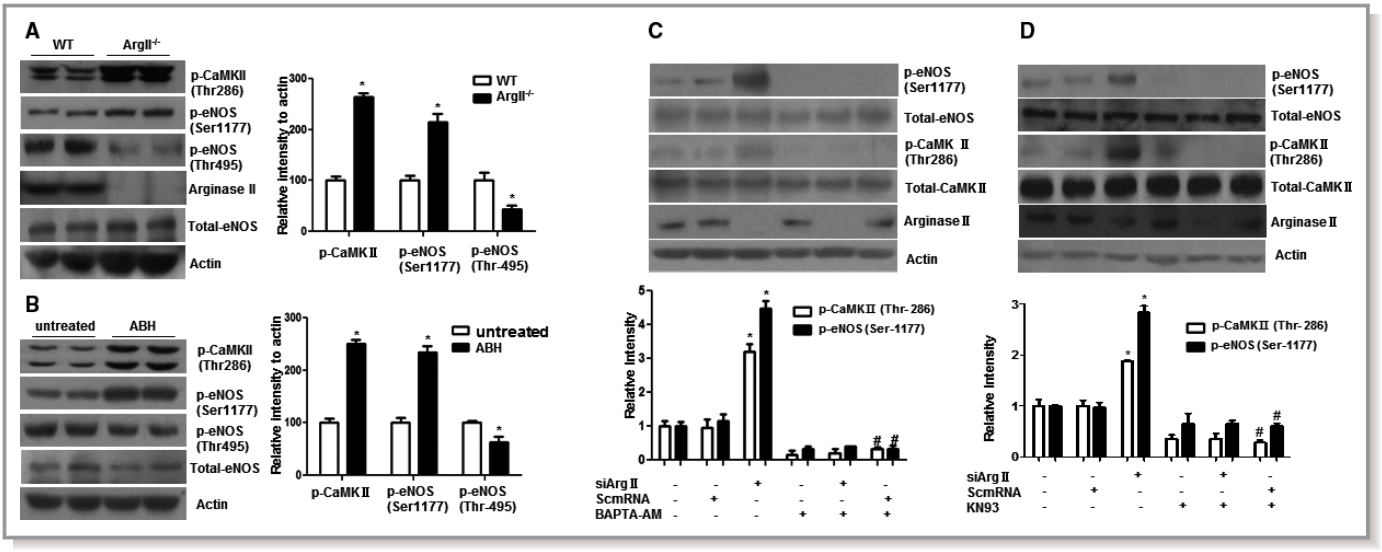

Figure 2. Downregulation of arginase II elicited an increase in CaMKII-dependent eNOS Ser1177 phosphorylation and a decrease in eNOS Thr495 phosphorylation. A, Aortic lysates were prepared from WT and $ArgII^{-/-}$ mice, and Western blot analyses were performed 9 (n=3 mice). B, HUVECs lysates treated with ABH were analyzed using Western blotting (n=3 experiments). C, HUVECs were incubated with siArgII and scmRNA (24 hours) and then treated with BAPTA-AM (10 μmol/L, 1 hour). Cell lysates were analyzed for the expression and phosphorylation of proteins. D, siRNA-incubated HUVECs were treated with KN-93 (1 μmol/L, 1 hour). Protein amounts and phosphorylation were analyzed (n=4 experiments). ABH indicates 2(S)-amino-6-boronohexanoic acid; CaMKII, Ca^{2+}/calmodulin-dependent protein kinase II; EC, endothelial cells; eNOS, endothelial nitric oxide synthase; HUVEC, human umbilical vein endothelial cells; siRNA, small interfering RNA; WT, wild-type. *vs WT, $P<0.05$, n=3 mice; #vs untreated, $P<0.01$.

−7.16±0.04 versus −7.12±0.19 mol/L, E_{max}, 86.75±1.48 versus 56.85±3.91%, $P<0.01$; log EC_{50}; $ApoE^{-/-}$+HCD versus $ApoE^{-/-}$+HCD+sip32, −7.12±0.19 versus −7.30 ±0.14 mol/L, E_{max}, 56.85±3.91 versus 92.25±4.42%, $P<0.01$) and attenuated PE-dependent vasoconstriction (Figure 7J, log EC_{50}; WT versus $ApoE^{-/-}$+HCD, −6.79±0.07 versus −7.06±0.19 mol/L, E_{max}, 135.90±4.33 versus 333.30±24.92%, $P<0.01$; log EC_{50}; $ApoE^{-/-}$+HCD versus $ApoE^{-/-}$+HCD+sip32, −7.06±0.19 versus −6.72±0. 25 mol/L, E_{max}, 333.30±24.92 versus 111.20±12.19%, $P<0.01$), however, sodium nitroprusside responses were the same in all groups (Figure 7I). As shown in Figure S7, fluorescent-labeled siRNAs were predominantly localized in the endothelia of aortic vessels.

Discussion

In the present study, we showed that arginase II inhibition decreased $[Ca^{2+}]m$ and increased $[Ca^{2+}]c$, resulting in CaMKII-dependent eNOS activation. The regulation of intracellular $[Ca^{2+}]$ by arginase II is p32-dependent. Arginase II activity controls the concentration of free SPM, a molecule binding to p32 and facilitating Ca^{2+} release from p32, and arginase II protein level controls p32 protein concentration. p32 knockdown with siRNA enhanced the Ca^{2+}/CaMKII/eNOS activation axis and improved endothelial dysfunction in $ApoE^{-/-}$ mice fed an HCD. The increase in $[Ca^{2+}]m$ caused by arginase II inhibition was not associated with enhanced NO production, as shown in the results from eNOS KO mice. Finally, we conclude that arginase II participates in endothelial dysfunction by contributing to the regulation of intracellular Ca^{2+} concentration in an NO-independent manner.

Two different mechanisms are responsible for the critical role of arginase II in p32-dependent intracellular $[Ca^{2+}]$ regulation between the cytosol and mitochondria. One mechanism involves arginase II activity that controls the concentration of free SPM, a key molecule inducing decreased eNOS-dependent NO release through augmented phosphorylation at Thr495 and attenuated phosphorylation at eNOS Ser1177 (Figure 4D). In the present study, SPM level was controlled by arginase activity in HUVECs with arginase downregulation, ABH, and siArgII, (Figure 5A) and in $ApoE^{-/-}$ mice fed an HCD with increased arginase activity (Figure 7B and 7C). Reportedly, intracellular SPM mostly binds to RNA, DNA, and phospholipids, as well as ATP at submillimolar levels (<mmol/L) and free SPM at μmol/L levels.[31] In our experiments, the measured SPM concentration was 18±3.4 μmol/L in HUVECs and 8±2.1 μmol/L in the aorta of WT mice. SPM, a biological polyamine, has various biological functions and can be taken up by mitochondria.[32] Among the polyamines, putrescine, spermidine, and SPM, only SPM with 4 amino groups induced an increase in p32-dependent $[Ca^{2+}]m$ (Figure 4C). This difference in polyamine activity is likely

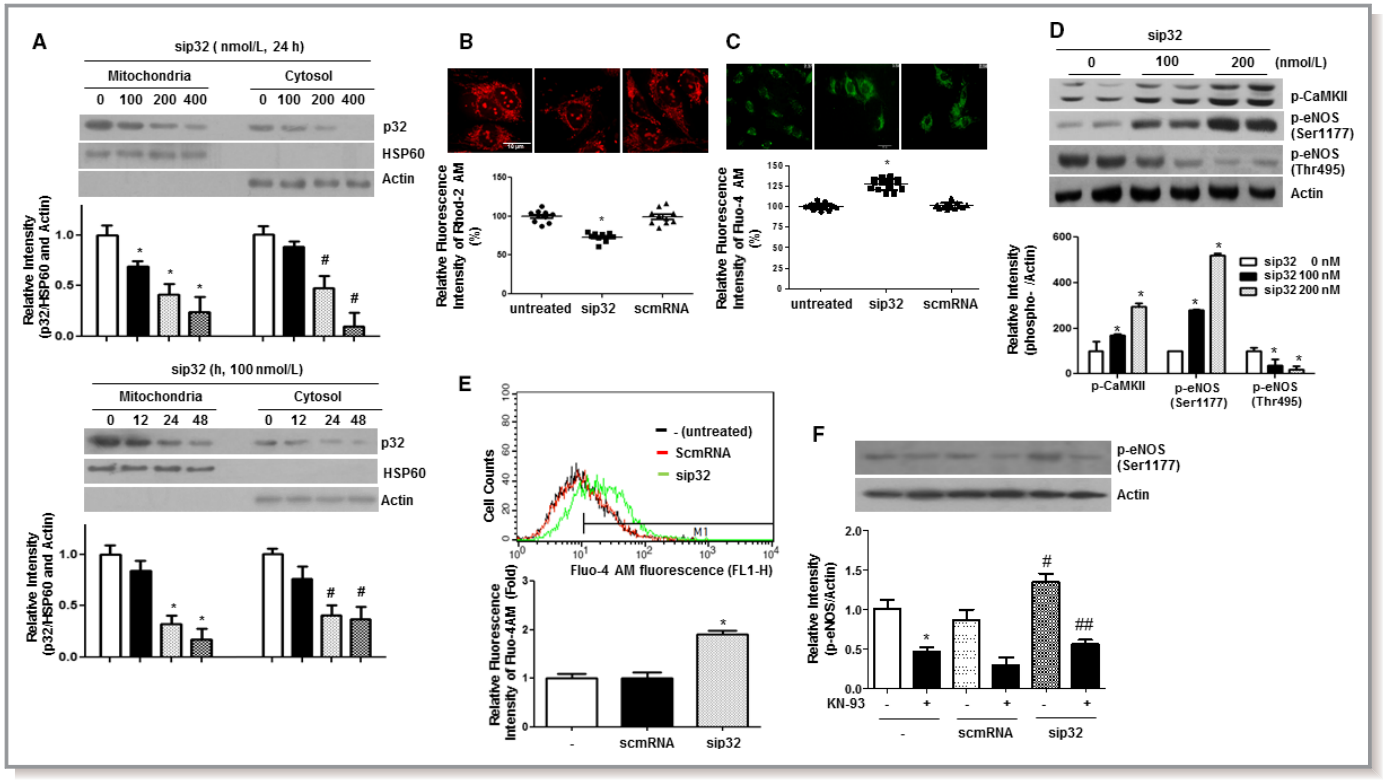

Figure 3. sip32-activated Ca^{2+}/CaMKII/eNOS axis phosphorylation. A, sip32 was incubated at different concentrations (top) and for different time periods (bottom), and the silencing efficacy was determined after mitochondrial fractionation. HSP60 and actin were used as marker proteins for the mitochondria and cytosol fraction, respectively (n=4 independent experiments).sip32 incubation (100 nmol/L, 24 hours) resulted in decreased $[Ca^{2+}]$m (B) and increased $[Ca^{2+}]$c (C) (n=12 to 15 images from 3 independent experiments). D, sip32 treatment (100 nmol/L, 24 hours) induced the phosphorylation of CaMKII and eNOS Ser1177, but decreased eNOS Thr495 phosphorylation (n=4 independent experiments). E, FACS analysis of sip32-treated HUVECs was performed to confirm the change in $[Ca^{2+}]$c. n=3 independent experiments. F, The effect of sip32 on eNOS Ser1177 phosphorylation was tested in the presence of CaMKII inhibitor (KN-93, 1 μmol/L, 1 hour) (n=3 independent experiments). CaMKII indicates Ca^{2+}/calmodulin-dependent protein kinase II; eNOS, endothelial nitric oxide synthase; HUVECs, human umbilical vein endothelial cells. *vs untreated, $P<0.05$; #vs untreated without siRNA, $P<0.05$; ##vs untreated with sip32, $P<0.05$.

attributable to the different polycationic structures of these compounds, which accounts for their flexibility and hydration. Because of the presence of 2 N atoms in the middle of the molecule, SPM is the most flexible of the 3 polyamines and has positive charges at fixed lengths along a conformationally flexible carbon chain, which can bridge critical distances.[33] As shown in MALDI-TOF analysis (Figure S2B), only SPM could bind to p32, at the ratio of 1:1. These SPM properties may affect the Ca^{2+}-binding capacity of p32 (Figure S2F and S2G). Fluorescence immunoassay (Figure S8) showed that only rhodamine B-tagged SPM bound to p32, with a dissociation constant (K_d) of 66.2±4.8 μmol/L. The high K_d value may be attributed to rhodamine B tag conjugated to one of the SPM amino groups. We also found that urea, a product of arginase reaction, had no effect on the Ca^{2+}-binding capacity of p32. The second mechanism is involved in the association of the arginase II protein level with p32 protein level observed in HUVECs treated with siArgII (Figure 5B) and in the aortas of $ArgII^{-/-}$ mice (Figure 5C), however, treatment of HUVECs with ABH and L-Arg had no effect on p32 protein level (Figure S4A and S4B). In the aortas of $ArgII^{-/-}$ mice, L-Arg and SPM concentrations were not changed (Figure 5D), however, decreased p32 expression, increased $[Ca^{2+}]$c, and increased eNOS Ser117 phosphorylation were observed. Furthermore, p32 protein level did not effect on arginase II protein level (Figure S4C) or arginase activity (Figure S4D). Therefore, these results suggested that arginase II protein may be involved in the regulation of p32 protein stability without affecting on protein synthesis because siArgII did not downregulated HSP60 protein level (Figure 5B) and siArgII did not also have an effect on mRNA level of p32 in quantitative real-time PCR (qRT-PCR) analysis. The regulation of p32 level apparently differs between humans and mice. In mice, increased arginase activity without a change of protein abundance[2] showed increased p32 level (Figure 7A and 7B). However, in HUVECs, arginase II protein level, not activity, was associated with p32 level (Figure S4A and S4C). Additionally, the half-life of p32 was ≈6 hours in cycloheximide-treated HUVECs. Therefore, arginase II plays an important role in mediating

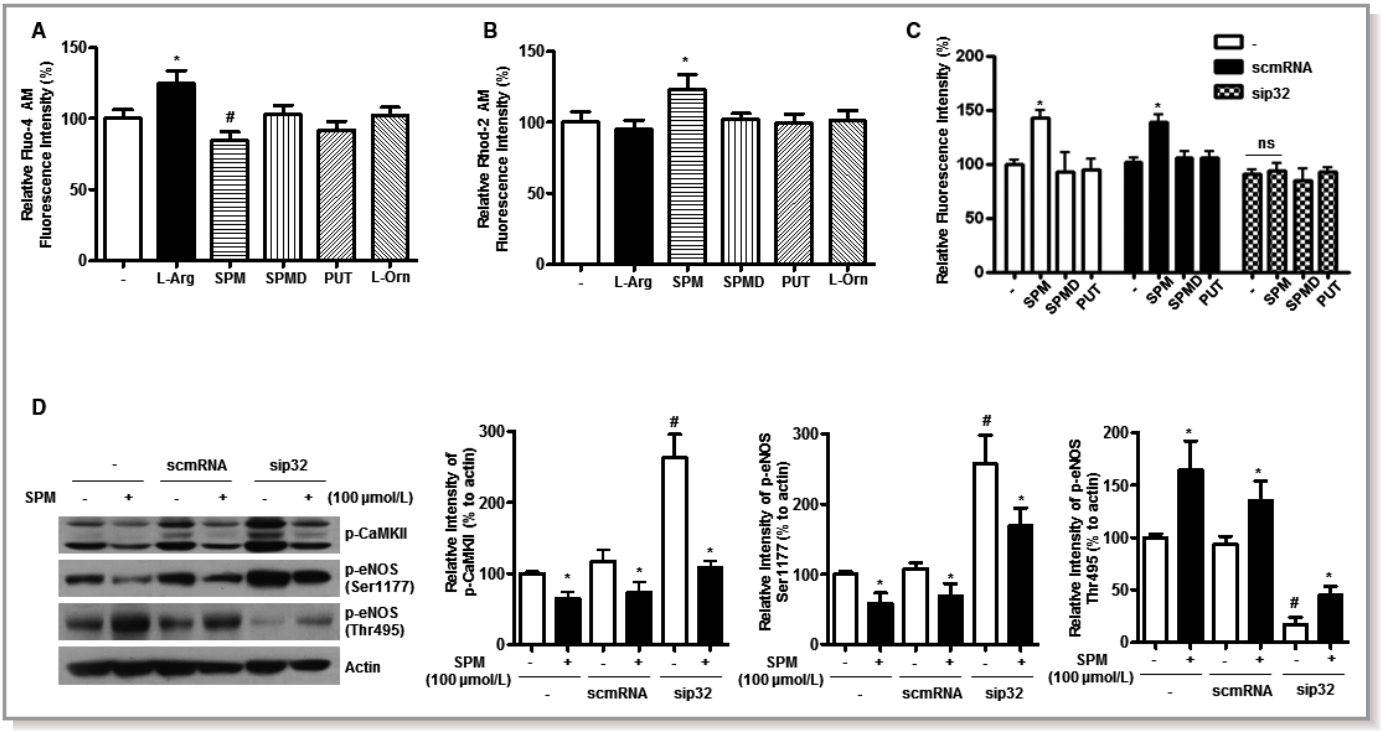

Figure 4. SPM bound to p32 and reduced eNOS Ser1177 phosphorylation. HUVECs were treated with L-Arg, SPM, SPMD, PUT, or L-ornithine at 10 mmol/L for 1 hour and stained with Fluo-4 AM (A) and Rhod-2 AM (B). Relative fluorescence intensities are presented as bar graphs (n=15 images from 3 independent experiments). C, HUVECs were incubated with sip32 and scmRNA for 24 hours and then treated with polyamine (each 100 μmol/L, 1 hour). Cells were stained with Rhod-2 AM to measure $[Ca^{2+}]$m. Relative Rhod-2 fluorescence intensities are shown as a bar graph (n=15 to 16 images from 4 different experiments). D, siRNA-treated HUVECs were incubated with SPM (100 μmol/L, 1 hour) and phosphorylation of CaMKII and eNOS was analyzed using Western blotting. The band intensities are shown as bar graphs (n=3 different experiments). CaMKII indicates Ca^{2+}/calmodulin-dependent protein kinase II; HUVECs, human umbilical vein endothelial cells; eNOS, endothelial nitric oxide synthase. *vs untreated, $P<0.05$; #vs SPM-untreated control, $P<0.05$; ##vs siRNA- and SPM-untreated control, $P<0.05$.

intracellular $[Ca^{2+}]$ between mitochondria and cytosol through a p32-dependent mechanism.

p32 has both mitochondrial and non-mitochondrial localization, although p32 predominantly targets to mitochondria with an N-terminal mitochondria-targeting sequence.[25] In this study, we have fractionated the cell lysate into mitochondria and cytosol and found that p32 was abundantly presented in the mitochondria. Interestingly, downregulation of [p32]m using sip32-targeting mitochondria-targeting sequence (Figure 3A) and upregulation of [p32]m in $ApoE^{-/-}$ mice fed an HCD (Figure 7B) showed decreased and increased [p32]c, respectively. These results suggest that [p32]c can be released from mitochondrial p32 during mitochondrial events. p32 silencing enhanced mitochondrial fission and the loss of mitochondrial fusion with the loss of detectable levels of Mfn1/2 proteins.[34] Additionally, the difference in molecular weight of p32 observed in Western blot and MALDI-TOF mass spectrometry analysis is probably because of glycosylation and strong charges.[35]

In the present study, we report a novel function of p32 in a Ca^{2+}-dependent eNOS regulation of ECs. Although how p32 regulates Ca^{2+} levels between cytosol and mitochondria remains unknown, we suggest several plausible explanations. First, p32 may regulate Ca^{2+} level if p32 directly forms a Ca^{2+} channel and a pore-like homotrimer,[29] indicating a plausible candidate for a permeability transition pore (PTP) channel.[36] Second, p32 may function as a mitochondrial Ca^{2+}-storage protein (Figure S2F). Further studies are necessary to test this hypothesis because currently we cannot explain why sip32 elicited an increase in $[Ca^{2+}]$c and CaMKII-dependent eNOS phosphorylation even though [p32]c was decreased. Third, released Ca^{2+} from p32 may activate the other Ca^{2+} channels in the mitochondria. We designed siRNA against the mitochondrial Ca^{2+} uniporter (accession No. NM_138357), however, the siRNA had no effect on $[Ca^{2+}]$m caused by arginase inhibition. In addition, siRNA knockdown of cyclophilin D, a prominent mediator of the mitochondrial permeability transition pore, did not show any effect on SPM-induced increase in $[Ca^{2+}]$m. Finally, we cannot exclude out the possibility that p32 in the cytosol may also act as a regulator of $[Ca^{2+}]$c.

Arginase activation was associated with increased $[Ca^{2+}]$m (Figure 7D), and arginase inhibition reversely enhanced increased $[Ca^{2+}]$c (Figure 1C and 1D) that was not from extracellular Ca^{2+} (Figure S1). The central role of cellular Ca^{2+}

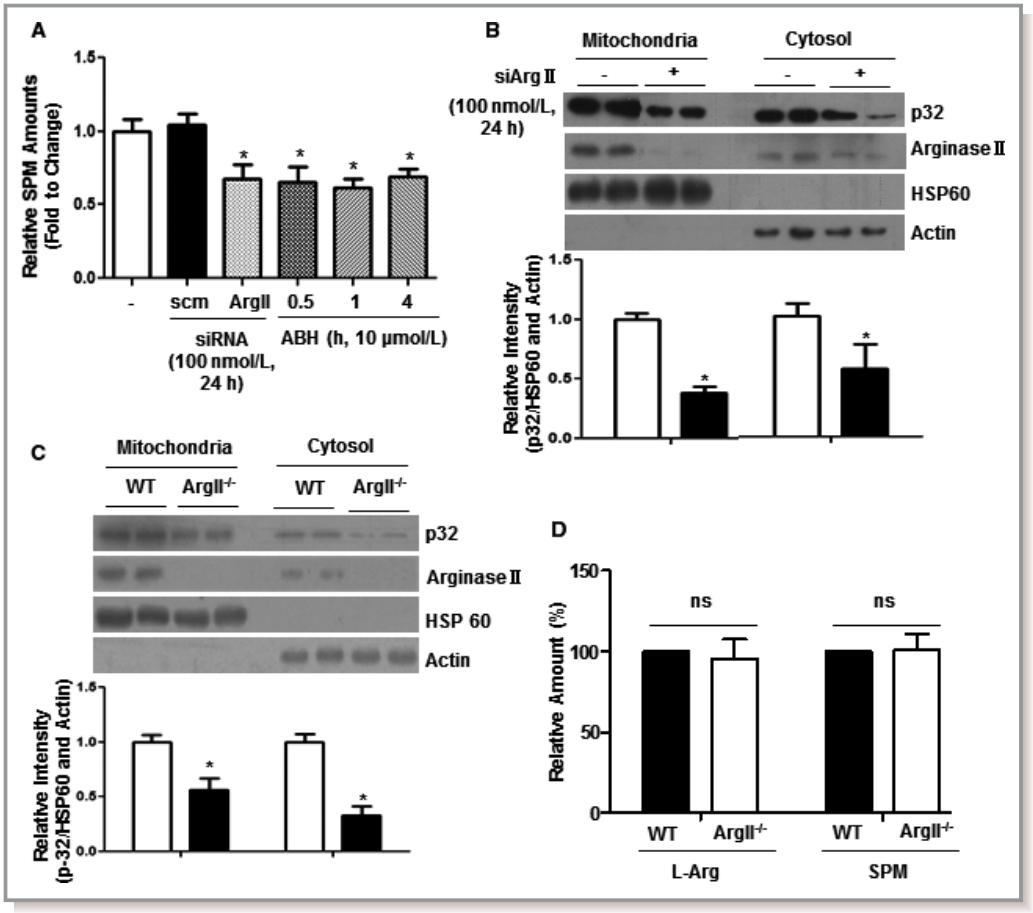

Figure 5. Arginase II inhibition reduced SPM level, and siArgII and gene knockout decreased p32 protein level. A, Intracellular SPM amounts were measured using HPLC in siRNA (siArgII and scmRNA)- and ABH-treated HUVECs., n=3 independent experiments. B, siArgII (100 nmol/L) were incubated with HUVECs for 24 hours, and p32 level was detected in both mitochondria and cytosol fractions using Western blot analysis. Detection of arginase II was used as a control for siArgII treatment (n=4 independent experiments). C, Aortas of WT and $ArgII^{-/-}$ mice were isolated, and mitochondria and cytosol fractions were separated. P32 and arginase II expression levels were detected (n=4 independent experiments from 4 mice). D, Aortic lysates from WT and $ArgII^{-/-}$ mice were analyzed using HPLC to L-Arg and SPM. ns, non-significant, n=4 independent experiments from 4 mice. HPLC indicates high performance liquid chromatography; HUVECs, human umbilical vein endothelial cells; siRNA, small interfering RNA; SPM, spermine; WT, wild-type. *vs WT, $P<0.01$.

homeostasis is controlled by the endoplasmic reticulum (ER), and mitochondria. First, mitochondrial Ca^{2+} uptake can activate several dehydrogenases (pyruvate dehydrogenase, isocitrate dehydrogenase, and α-ketoglutarate dehydrogenase) in the matrix and elevate the respiration rate and ATP production.[37] Consistently, arginase inhibition and sip32 treatment reduced intracellular ATP level (Figure S9). However, a prolonged increase in $[Ca^{2+}]$m can induce mitochondrial swelling, cytochrome C release, and apoptotic cell death.[38] In addition to altering the mitochondrial activity, increased $[Ca^{2+}]$c played an important role in eNOS activation through CaM and CaMKII in vascular ECs. CaM binds to a CaM-binding motif that inhibits Thr495 phosphorylation and then facilitates NADPH-dependent electron flow from the reductase domain to the oxygenase domain by displacing an adjacent autoinhibitory loop of eNOS. CaMKII mediates Ser1177 phosphorylation in the reductase domain, and then NO production is increased by enhancing the electron flux through the reductase domain.[39] Therefore, arginase activity adjusts the phosphorylation of 2 important amino acids, Ser1177 and Thr495, when eNOS is activated through a Ca^{2+}-dependent mechanism.

NO generated by eNOS increases mitochondrial biogenesis and enhances respiration and ATP content.[40] Reciprocally, arginase inhibition increased NO production, and L-Arg supplementation increased $[Ca^{2+}]$c (Figure 4A). Therefore, we investigated the effect of arginase inhibition on $[Ca^{2+}]$m in $eNOS^{-/-}$ mice to clearly demonstrate arginase inhibition

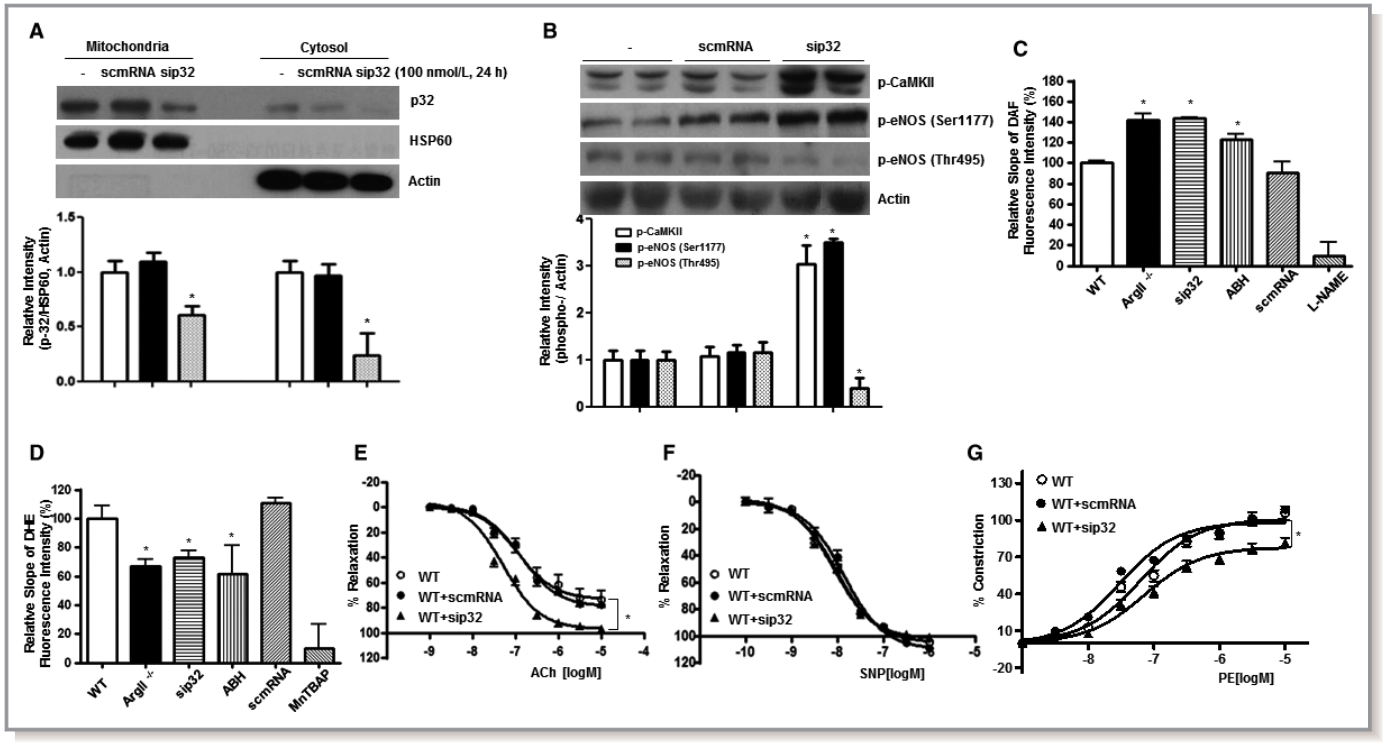

Figure 6. sip32-induced NO-dependent vasorelaxation in the aortas of WT mice. A, Aortic segments from WT mice were incubated with siRNA (final concentration,100 nmol/L) for 24 hours. p32 level was detected using Western blot analysis after mitochondrial fractionation (n=4 independent experiments from 4 mice). B, Aortas of WT mice were treated with siRNA, and proteins phosphorylation was analyzed using Western blotting (n=3 independent experiments from 3 mice). NO production (C) and ROS generation (D) were measured as time-dependent changes in DAF (4-amino-5-methylamino-2',7'-difluorofluorescein) and DHE (dihydroethidine) fluorescence intensities, respectively. The slopes were defined as the change in fluorescence intensity, and relative slopes are presented as a bar graph. siRNA and ABH (2(S)-amino-6-boronohexanoic acid) were incubated with aortas for 24 hours. NG-nitro-L-arginine methyl ester (100 μmol/L) was used as a control (n=8 aortic segments from 4 mice). Endothelium-dependent vasorelaxation responses to A (E), endothelium-independent relaxation responses to SNP (F), and contractile responses to PE (G) were determined using siRNA-treated aortas (n=8 aortas from 4 mice). NO indicates nitric oxide; ROS, reactive oxygen species; siRNA, small interfering RNA; WT, wild-type. *vs untreated, $P<0.01$.

effects. As shown in Figure S3, arginase inhibition with ABH-induced CaMKII phosphorylation, and arginase II and mitochondrial p32 expressions were significantly augmented (A and B). Consistent with previous results, $[Ca^{2+}]$m in ECs from $eNOS^{-/-}$ mice was increased compared with that of WT mice, which was reduced by the arginase inhibitor, ABH, comparable to ECs from $ArgII^{-/-}$ mice (C). Therefore, Ca^{2+}/CaMKII/eNOS axis phosphorylation caused by arginase inhibition was attributed not to increase NO production, but to arginase-dependent p32 regulation.

Uncoupled eNOS is an important ROS-producing enzyme contributing to atherogenesis in HCD-fed $ApoE^{-/-}$ mice. As shown in Figure S10, increased ROS production in HCD-fed $ApoE^{-/-}$ mice was attenuated with treatment of NG-nitro-L-arginine methyl ester, ABH, sip32, and diphenyleneiodonium (DPI, NADPH oxidase inhibitor). These data indicate that NADPH oxidase and uncoupled eNOS are major sources for ROS production in atherogenesis. Several mechanisms have been implicated in eNOS uncoupling under pathophysiological conditions, including: (1) L-arginine depletion; (2) cofactor depletion; (3) altered eNOS phosphorylation; and (4) protein-protein interactions among Ca^{2+}/calmodulin, caveolin, and HSP90.

Our results indicate that arginase II-dependent p32 activity in endothelial mitochondria can modulate the intracellular concentrations of ROS, NO and Ca^{2+}, which are responsible for endothelial function. Therefore, herein, we present a novel mechanism showing that arginase II can modulate mitochondrial function associated with endothelial function through p32–dependent Ca^{2+} regulation by two mechanisms, one dependent on L-Arg and the other associated with p32.

In conclusion, p32 activity regulated by arginase II, SPM concentration, and p32 expression, altered $[Ca^{2+}]$ in both mitochondria and cytosol. Downregulation of arginase II and p32 enhanced the Ca^{2+}/CaMKII/eNOS axis, and sip32 restored endothelial dysfunction in $ApoE^{-/-}$ mice fed an HCD. These results underly a novel mechanism for arginase–dependent constriction of eNOS activity. In this study, p32 was identified as a new therapeutic target for vascular disorders such as atherosclerosis in which NO production was

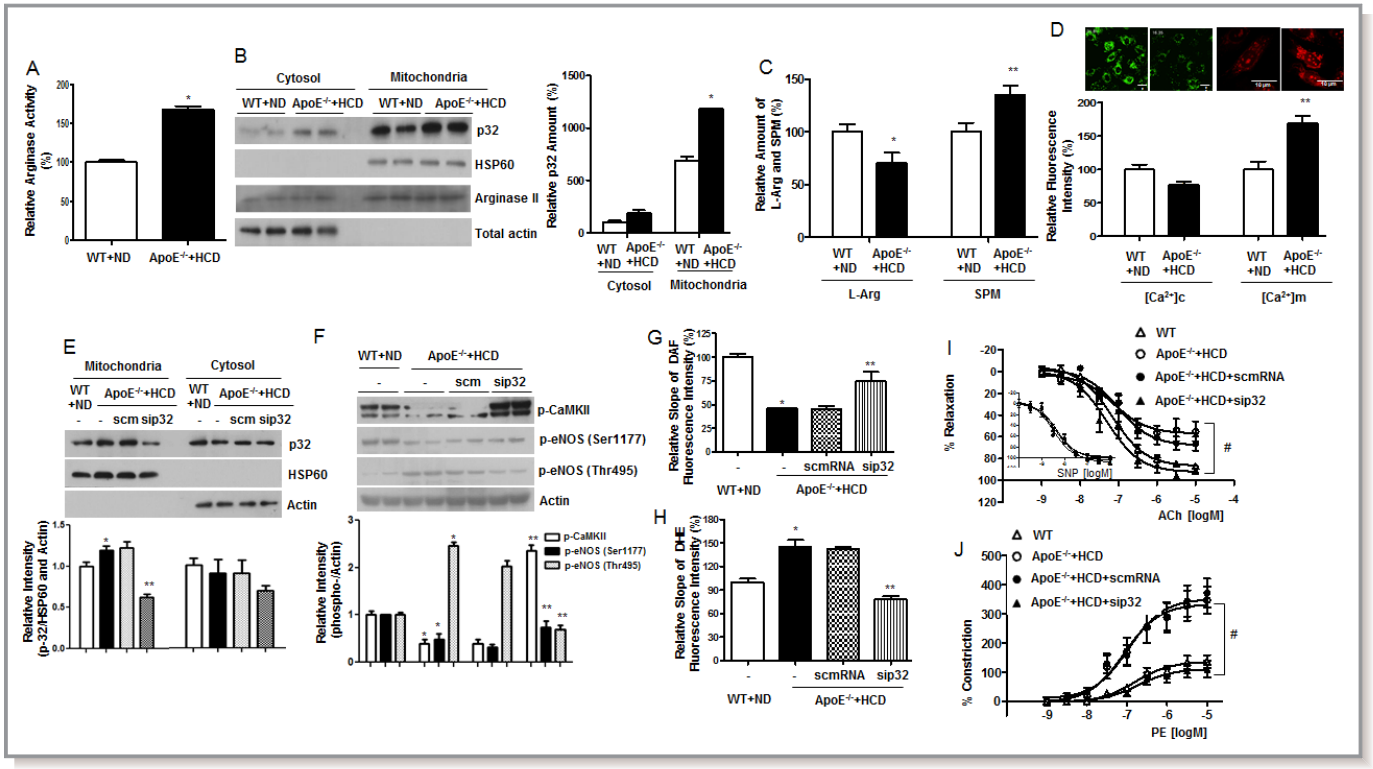

Figure 7. Increased mitochondrial p32 level in the aortas of ApoE$^{-/-}$ mice fed an HCD showed increased [Ca^{2+}]m and decreased [Ca^{2+}]c that was reversed by sip32. A, WT and ApoE$^{-/-}$ mice were fed an ND and HCD, and arginase activities were measured in isolated aortas (n=3 experiments from 3 mice). B, Mitochondria were fractionated from cytosol with aortic tissue, and p32 level was determined. Relative p32 levels are shown as a bar graph (n=4 experiments from 4 mice). C, Aortic intracellular L-Arg and SPM levels were analyzed using HPLC and are presented as relative amounts (n=4 experiments from 4 mice). D, Aortic endothelial cells were isolated from WT and ApoE$^{-/-}$ mice fed an ND and HCD and stained with Fluo-4 AM (top) and Rhod-2 AM (bottom) to determine [Ca^{2+}]c and [Ca^{2+}]m, respectively. Fluorescence intensities are presented as a bar graph (n=15 images from 3 mice). E, WT and ApoE$^{-/-}$ mice were fed an ND and HCD and siRNAs were administered by intravenous injection 5 times before the experiment. The p32 protein level was determined after mitochondrial fractionation (n=3 experiments from 3 mice). F, Protein phosphorylation was analyzed using Western blotting (n=4 experiments from 4 mice). NO (G) and ROS (H) production in aortic endothelia was determined using DAF and DHE fluorescence dyes, and the slopes are presented as a bar graph (n=6 experiments from 3 mice). I, Vasodilator dose responses to Ach and SNP (inset) in the aortas of WT+ND and ApoE$^{-/-}$+HCD injected with siRNAs were determined (n=12 from 3 mice). J, Dose-response effects of PE on vascular constriction were then determined (n=12 from 3 mice). DAF indicates 4-amino-5-methylamino-2′,7′-difluorofluorescein; DHE, dihydroethidine; HCD, high cholesterol diet; HPLC, high performance liquid chromatography; ND, normal diet; ROS, reactive oxygen species; siRNA, small interfering RNA; sip32, siRNA against p32; SPM, spermine; WT, wild-type.*vs WT+ND, $P<0.01$; **vs WT+ND with SPM; $^{\#\#}$ApoE$^{-/-}$+HCD vs ApoE$^{-/-}$+HCD+sip32, $P<0.01$.

interrupted and injurious ROS generation was promoted by endothelial dysfunction.

Acknowledgments

We thank Jaye P.F. Chin-Dusting (Monash Biomedicine Discovery Institute, Melbourne, Australia) for the generous gift of the Arginase II KO mice and for the agreement and the central laboratory of Kangwon National University for technical assistance for instruments.

Sources of Funding

This work was supported by the Basic Science Research Program of the National Research Foundation of Korea funded by the Ministry of Education, Science and Technology (2015M3A9B6066968 and 2016M3A9B6903185 to Ryoo, 2014R1A6A1029617 to Jeon).

Disclosures

None.

References

1. Li H, Forstermann U. Prevention of atherosclerosis by interference with the vascular nitric oxide system. *Curr Pharm Des*. 2009;15:3133–3145.
2. Ryoo S, Gupta G, Benjo A, Lim HK, Camara A, Sikka G, Lim HK, Sohi J, Santhanam L, Soucy K, Tuday E, Baraban E, Ilies M, Gerstenblith G, Nyhan D, Shoukas A, Christianson DW, Alp NJ, Champion HC, Huso D, Berkowitz DE. Endothelial arginase II: a novel target for the treatment of atherosclerosis. *Circ Res*. 2008;102:923–932.
3. Haraguchi Y, Takiguchi M, Amaya Y, Kawamoto S, Matsuda I, Mori M. Molecular cloning and nucleotide sequence of cdna for human liver arginase. *Proc Natl Acad Sci USA*. 1987;84:412–415.

4. Morris SM Jr, Bhamidipati D, Kepka-Lenhart D. Human type II arginase: sequence analysis and tissue-specific expression. *Gene*. 1997;193:157–161.
5. Chang CI, Liao JC, Kuo L. Arginase modulates nitric oxide production in activated macrophages. *Am J Physiol*. 1998;274:H342–H348.
6. Ignarro LJ, Buga GM, Wei LH, Bauer PM, Wu G, del Soldato P. Role of the arginine-nitric oxide pathway in the regulation of vascular smooth muscle cell proliferation. *Proc Natl Acad Sci USA*. 2001;98:4202–4208.
7. Li H, Meininger CJ, Hawker JR Jr, Haynes TE, Kepka-Lenhart D, Mistry SK, Morris SM Jr, Wu G. Regulatory role of arginase I and II in nitric oxide, polyamine, and proline syntheses in endothelial cells. *Am J Physiol Endocrinol Metab*. 2001;280:E75–E82.
8. Morris SM Jr, Kepka-Lenhart D, Chen LC. Differential regulation of arginases and inducible nitric oxide synthase in murine macrophage cells. *Am J Physiol*. 1998;275:E740–E747.
9. Louis CA, Reichner JS, Henry WL Jr, Mastrofrancesco B, Gotoh T, Mori M, Albina JE. Distinct arginase isoforms expressed in primary and transformed macrophages: regulation by oxygen tension. *Am J Physiol*. 1998;274:R775–R782.
10. Collado B, Sanchez-Chapado M, Prieto JC, Carmena MJ. Hypoxia regulation of expression and angiogenic effects of vasoactive intestinal peptide (VIP) and VIP receptors in Incap prostate cancer cells. *Mol Cell Endocrinol*. 2006;249:116–122.
11. Berkowitz DE, White R, Li D, Minhas KM, Cernetich A, Kim S, Burke S, Shoukas AA, Nyhan D, Champion HC, Hare JM. Arginase reciprocally regulates nitric oxide synthase activity and contributes to endothelial dysfunction in aging blood vessels. *Circulation*. 2003;108:2000–2006.
12. Hein TW, Zhang C, Wang W, Chang CI, Thengchaisri N, Kuo L. Ischemia-reperfusion selectively impairs nitric oxide-mediated dilation in coronary arterioles: counteracting role of arginase. *FASEB J*. 2003;17:2328–2330.
13. Jung C, Gonon AT, Sjoquist PO, Lundberg JO, Pernow J. Arginase inhibition mediates cardioprotection during ischaemia-reperfusion. *Cardiovasc Res*. 2010;85:147–154.
14. Zhang C, Hein TW, Wang W, Miller MW, Fossum TW, McDonald MM, Humphrey JD, Kuo L. Upregulation of vascular arginase in hypertension decreases nitric oxide-mediated dilation of coronary arterioles. *Hypertension*. 2004;44:935–943.
15. Johnson FK, Johnson RA, Peyton KJ, Durante W. Arginase inhibition restores arteriolar endothelial function in dahl rats with salt-induced hypertension. *Am J Physiol Regul Integr Comp Physiol*. 2005;288:R1057–R1062.
16. Peyton KJ, Ensenat D, Azam MA, Keswani AN, Kannan S, Liu XM, Wang H, Tulis DA, Durante W. Arginase promotes neointima formation in rat injured carotid arteries. *Arterioscler Thromb Vasc Biol*. 2009;29:488–494.
17. Pandey D, Bhunia A, Oh YJ, Chang F, Bergman Y, Kim JH, Serbo J, Boronina TN, Cole RN, Van Eyk J, Remaley AT, Berkowitz DE, Romer LH. Oxldl triggers retrograde translocation of arginase2 in aortic endothelial cells via rock and mitochondrial processing peptidase. *Circ Res*. 2014;115:450–459.
18. Hwang HM, Lee JH, Min BS, Jeon BH, Hoe KL, Kim YM, Ryoo S. A novel arginase inhibitor derived from scutellavia indica restored endothelial function in apoe-null mice fed a high-cholesterol diet. *J Pharmacol Exp Ther*. 2015;355:57–65.
19. Koo BH, Yi BG, Jeong MS, Kwon SH, Hoe KL, Kwon YG, Won MH, Kim YM, Ryoo S. Arginase II inhibition prevents interleukin-8 production through regulation of p38 MAPK phosphorylation activated by loss of mitochondrial membrane potential in nLDL-stimulated hAoSMCs. *Exp Mol Med*. 2018;50:e438.
20. Fleming I, Fisslthaler B, Dimmeler S, Kemp BE, Busse R. Phosphorylation of Thr (495) regulates Ca(2+)/calmodulin-dependent endothelial nitric oxide synthase activity. *Circ Res*. 2001;88:E68–E75.
21. Salerno JC, Harris DE, Irizarry K, Patel B, Morales AJ, Smith SM, Martasek P, Roman LJ, Masters BS, Jones CL, Weissman BA, Lane P, Liu Q, Gross SS. An autoinhibitory control element defines calcium-regulated isoforms of nitric oxide synthase. *J Biol Chem*. 1997;272:29769–29777.
22. Lobaton CD, Vay L, Hernandez-Sanmiguel E, Santodomingo J, Moreno A, Montero M, Alvarez J. Modulation of mitochondrial Ca(2+) uptake by estrogen receptor agonists and antagonists. *Br J Pharmacol*. 2005;145:862–871.
23. Muta T, Kang D, Kitajima S, Fujiwara T, Hamasaki N. P32 protein, a splicing factor 2-associated protein, is localized in mitochondrial matrix and is functionally important in maintaining oxidative phosphorylation. *J Biol Chem*. 1997;272:24363–24370.
24. Krainer AR, Mayeda A, Kozak D, Binns G. Functional expression of cloned human splicing factor SF2: homology to RNA-binding proteins, U1 70K, and Drosophila splicing regulators. *Cell*. 1991;66:383–394.
25. Ghebrehiwet B, Lim BL, Peerschke EI, Willis AC, Reid KB. Isolation, cDNA cloning, and overexpression of a 33-kD cell surface glycoprotein that binds to the globular "heads" of C1q. *J Exp Med*. 1994;179:1809–1821.
26. Itahana K, Zhang Y. Mitochondrial p32 is a critical mediator of ARF-induced apoptosis. *Cancer Cell*. 2008;13:542–553.
27. Sunayama J, Ando Y, Itoh N, Tomiyama A, Sakurada K, Sugiyama A, Kang D, Tashiro F, Gotoh Y, Kuchino Y, Kitanaka C. Physical and functional interaction between BH3-only protein Hrk and mitochondrial pore-forming protein p32. *Cell Death Differ*. 2004;11:771–781.
28. Fogal V, Richardson AD, Karmali PP, Scheffler IE, Smith JW, Ruoslahti E. Mitochondrial p32 protein is a critical regulator of tumor metabolism via maintenance of oxidative phosphorylation. *Mol Cell Biol*. 2010;30:1303–1318.
29. Jiang J, Zhang Y, Krainer AR, Xu RM. Crystal structure of human p32, a doughnut-shaped acidic mitochondrial matrix protein. *Proc Natl Acad Sci USA*. 1999;96:3572–3577.
30. Boger RH, Bode-Boger SM, Mugge A, Kienke S, Brandes R, Dwenger A, Frolich JC. Supplementation of hypercholesterolaemic rabbits with l-arginine reduces the vascular release of superoxide anions and restores no production. *Atherosclerosis*. 1995;117:273–284.
31. Yan DH, Nishimura K, Yoshida K, Nakahira K, Ehara T, Igarashi K, Ishihara K. Different intracellular polyamine concentrations underlie the difference in the inward rectifier K(+) currents in atria and ventricles of the guinea-pig heart. *J Physiol*. 2005;563:713–724.
32. Toninello A, Miotto G, Siliprandi D, Siliprandi N, Garlid KD. On the mechanism of spermine transport in liver mitochondria. *J Biol Chem*. 1988;263:19407–19411.
33. Dalla Via L, Di Noto V, Siliprandi D, Toninello A. Spermine binding to liver mitochondria. *Biochim Biophys Acta*. 1996;1284:247–252.
34. Hu M, Crawford SA, Henstridge DC, Ng IH, Boey EJ, Xu Y, Febbraio MA, Jans DA, Bogoyevitch MA. P32 protein levels are integral to mitochondrial and endoplasmic reticulum morphology, cell metabolism and survival. *Biochem J*. 2013;453:381–391.
35. Robles-Flores M, Rendon-Huerta E, Gonzalez-Aguilar H, Mendoza-Hernandez G, Islas S, Mendoza V, Ponce-Castaneda MV, Gonzalez-Mariscal L, Lopez-Casillas F. P32 (gC1qBP) is a general protein kinase C (PKC)-binding protein; interaction and cellular localization of P32-PKC complexes in ray hepatocytes. *J Biol Chem*. 2002;277:5247–5255.
36. Starkov AA. The molecular identity of the mitochondrial Ca2+ sequestration system. *FEBS J*. 2010;277:3652–3663.
37. McCormack JG, Denton RM. The role of Ca2+ ions in the regulation of intramitochondrial metabolism and energy production in rat heart. *Mol Cell Biochem*. 1989;89:121–125.
38. Giorgi C, Romagnoli A, Pinton P, Rizzuto R. Ca2+ signaling, mitochondria and cell death. *Curr Mol Med*. 2008;8:119–130.
39. Fleming I, Busse R. Molecular mechanisms involved in the regulation of the endothelial nitric oxide synthase. *Am J Physiol Regul Integr Comp Physiol*. 2003;284:R1–R12.
40. Abelson JF, Kwan KY, O'Roak BJ, Baek DY, Stillman AA, Morgan TM, Mathews CA, Pauls DL, Rasin MR, Gunel M, Davis NR, Ercan-Sencicek AG, Guez DH, Spertus JA, Leckman JF, Dure LS IV, Kurlan R, Singer HS, Gilbert DL, Gilbert DL, Farhi A, Louvi A, Lifton RP, Sestan N, State MW. Sequence variants in SLITRK1 are associated with Tourette's syndrome. *Science*. 2005;310:317–320.

SUPPLEMENTAL MATERIAL

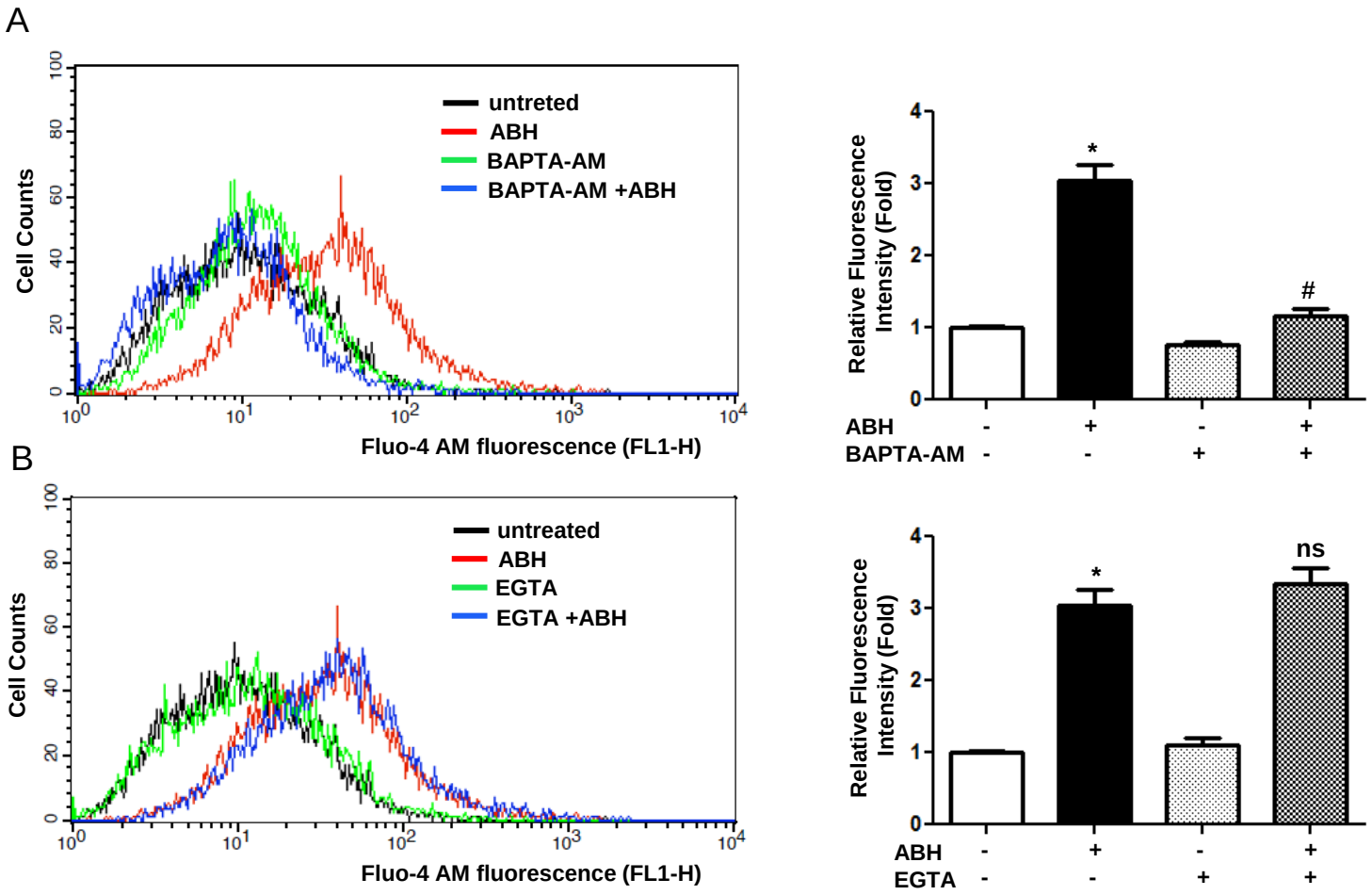

Figure S1. BAPTA-AM, not EGTA, blocked the increase in $[Ca^{2+}]c$ induced by arginase inhibition. HUVECs were incubated with intracellular and extracellular Ca^{2+}-chelating agents, BAPTA-AM (10 μmol/L, 30 min) (A) and EGTA (10 μmol/L, 30 min) (B), respectively. Cells were treated with the arginase inhibitor ABH and stained with Fluo-4 AM (1 mol/LM, 1 h). Fluorescence intensity was analyzed using FACS and presented as bar graphs. * vs. untreated control, $p<0.01$; # vs. ABH, $p<0.01$. ns, non-significant to ABH; n=4 independent experiments. HUVECs, human umbilical vein endothelial cells, BAPTA-AM, 1,2-Bis(2-aminophenoxy)ethane-*N*,*N*,*N*',*N*'-tetraacetic acid tetrakis(acetoxymethyl ester), EGTA, 3,12-bis(carboxymethyl)-6,9-dioxa-3,12-diazatetradecanedioic acid, FACS, fluorescence activated cell sorter.

A

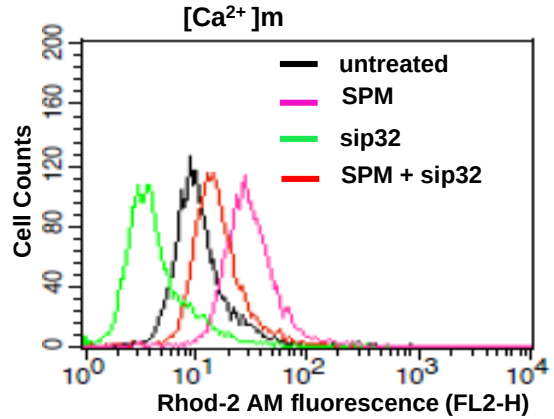
[Ca2+]m
untreated
SPM
sip32
SPM + sip32
Cell Counts
Rhod-2 AM fluorescence (FL2-H)

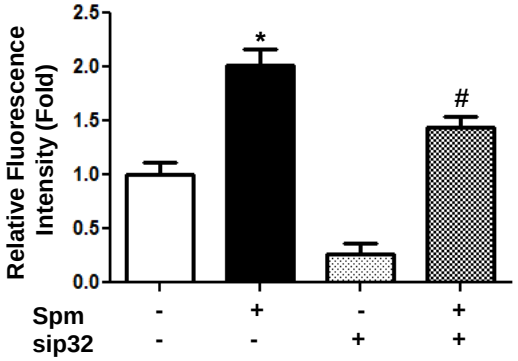
Relative Fluorescence Intensity (Fold)
Spm
sip32

B

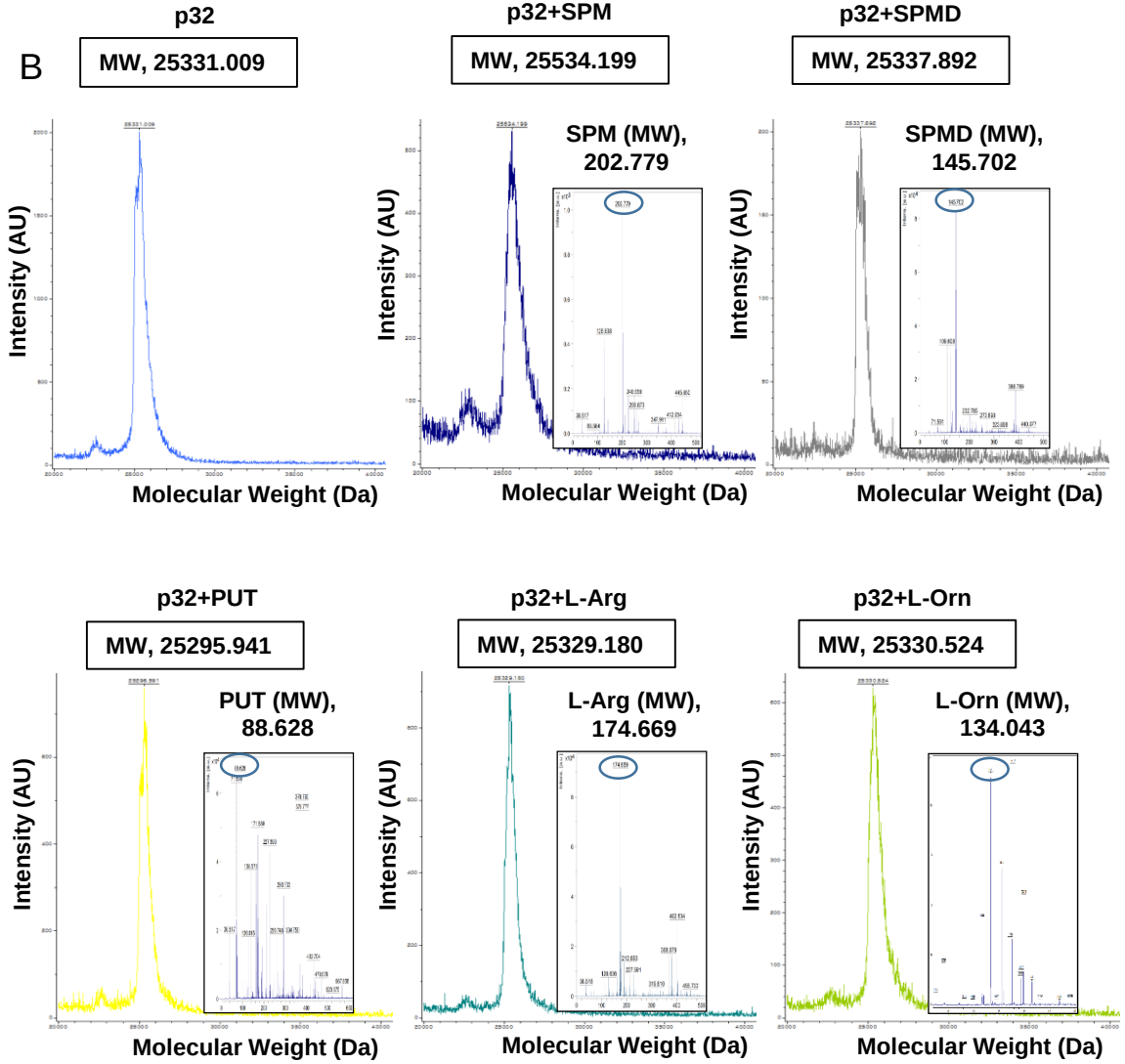
p32
MW, 25331.009
p32+SPM
MW, 25534.199
SPM (MW), 202.779
p32+SPMD
MW, 25337.892
SPMD (MW), 145.702
p32+PUT
MW, 25295.941
PUT (MW), 88.628
p32+L-Arg
MW, 25329.180
L-Arg (MW), 174.669
p32+L-Orn
MW, 25330.524
L-Orn (MW), 134.043
Intensity (AU)
Molecular Weight (Da)

C

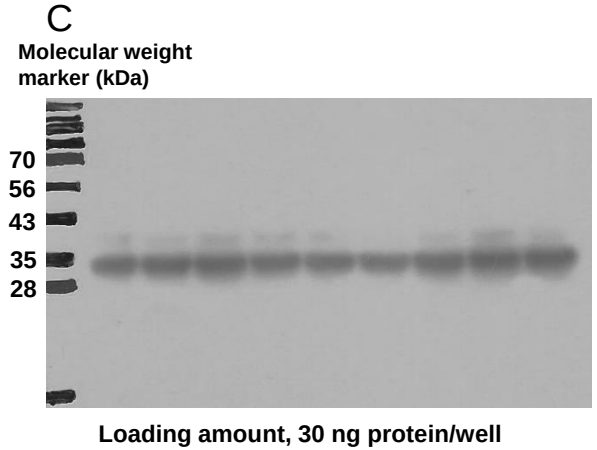
Molecular weight marker (kDa)
70
56
43
35
28
Loading amount, 30 ng protein/well

D

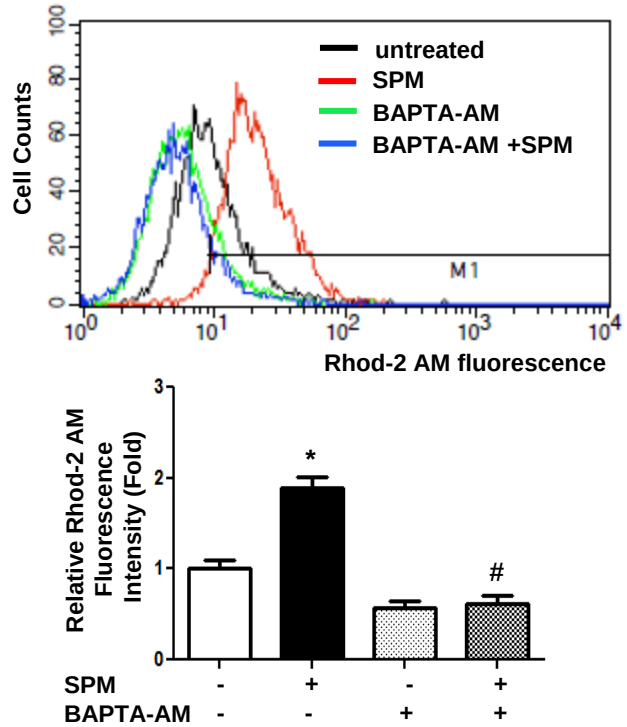
untreated
SPM
BAPTA-AM
BAPTA-AM +SPM
Cell Counts
M1
Rhod-2 AM fluorescence
Relative Rhod-2 AM Fluorescence Intensity (Fold)
SPM
BAPTA-AM

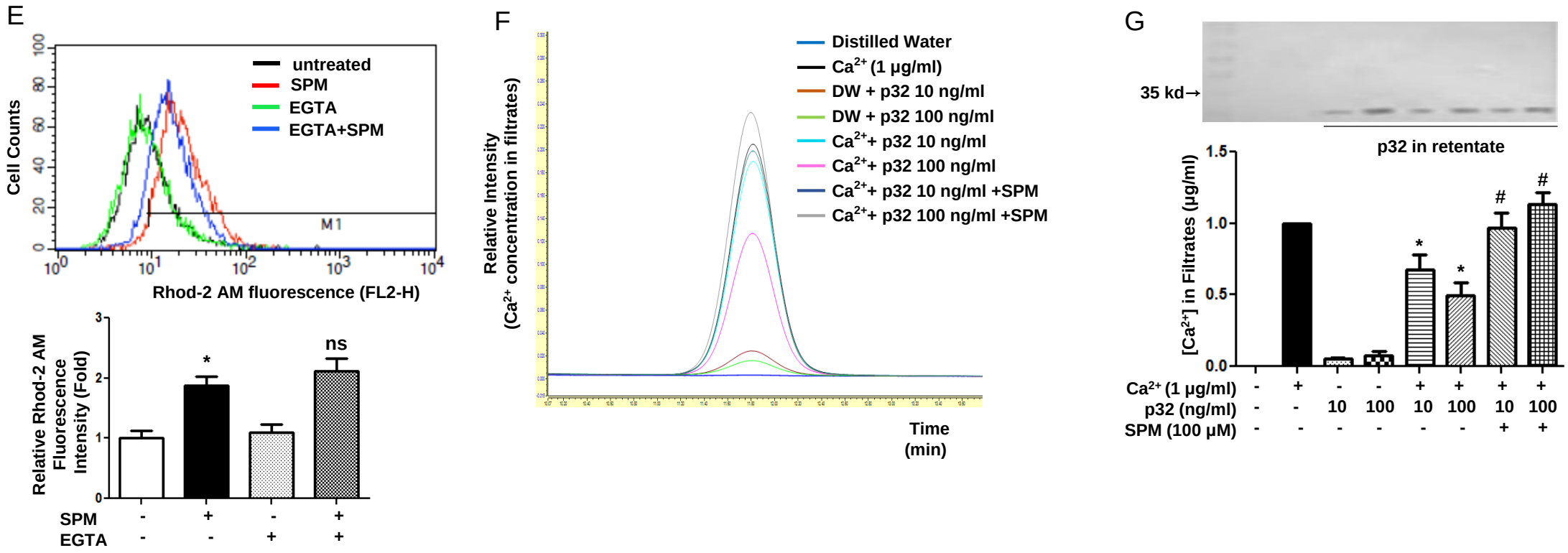

Figure S2. Spermine (SPM) interacted with p32 and blocked Ca^{2+} binding capacity of p32.
sip32 prevented SPM-induced increase in $[Ca^{2+}]m$ (A). * vs. untreated, $p<0.01$; # vs. SPM, $p<0.01$, n=4 independent experiments. To confirm the direct interaction between p32 and SPM, MALDI-TOF analysis was performed. The molecular weight (MW) of p32 was increased only in SPM-treated p32 (B), n=3 independent experiments. (C) Western blot analysis was performed to determine the MW of p32 because the MW of p32 was low in MALDI-TOF analysis. The data indicated that the MW of p32 is 32 kDa (n=2 experiments). SPM-induced increase in $[Ca^{2+}]m$ was prevented with BAPTA-AM (10 μmol/L, 30 min) (D), but not with EGTA (E, 10 μmol/L, 30 min). * vs. untreated, $p<0.01$; # vs. SPM, $p<0.01$, ns, not significant to SPM, n=3 independent experiments. Ion chromatography was performed to determine the binding capacity of p32 to Ca^{2+} ions (Methods section). SPM preincubation inhibited dose-dependent Ca^{2+} binding to p32. Representative chromatogram (F) and Ca^{2+} concentration in filtrate (free Ca^{2+}) are shown as a bar graph (G). * vs. Ca^{2+} only, $p<0.01$; # vs. p32+Ca^{2+}, $p<0.01$, n=3 independent experiments. sip32, small interfering RNA against p32, MALDI-TOF, matrix-assisted laser desorption ionization time of flight, $[Ca^{2+}]m$, mitochondrial Ca^{2+} level.

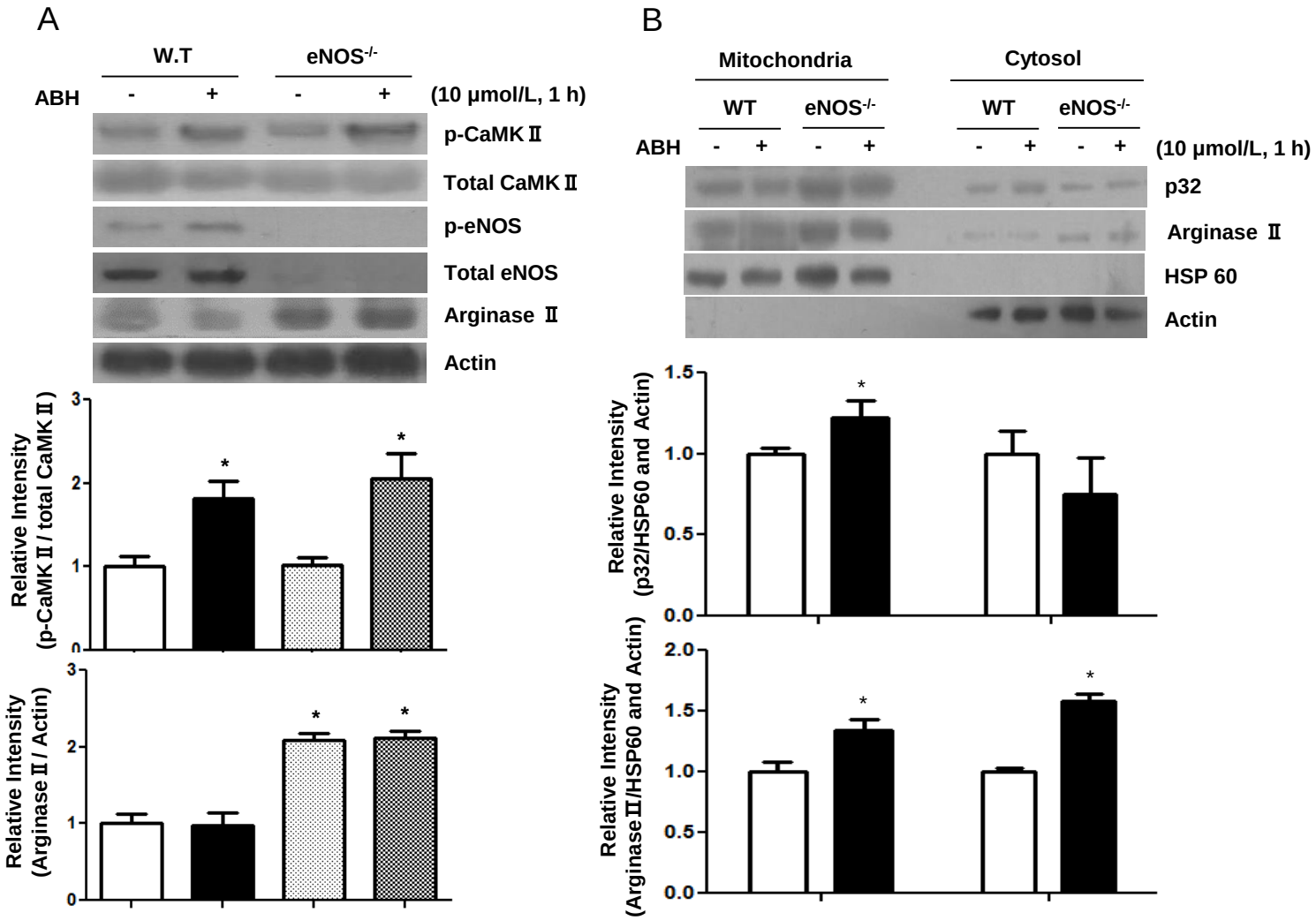
A
W.T
eNOS-/-
ABH
- + - +
(10 μmol/L, 1 h)
p-CaMKⅡ
Total CaMKⅡ
p-eNOS
Total eNOS
Arginase Ⅱ
Actin
Relative Intensity (p-CaMKⅡ/ total CaMKⅡ)
Relative Intensity (Arginase Ⅱ/ Actin)
B
Mitochondria
Cytosol
WT
eNOS-/-
WT
eNOS-/-
ABH
- + - + - + - +
(10 μmol/L, 1 h)
p32
Arginase Ⅱ
HSP 60
Actin
Relative Intensity (p32/HSP60 and Actin)
Relative Intensity (ArginaseⅡ/HSP60 and Actin)

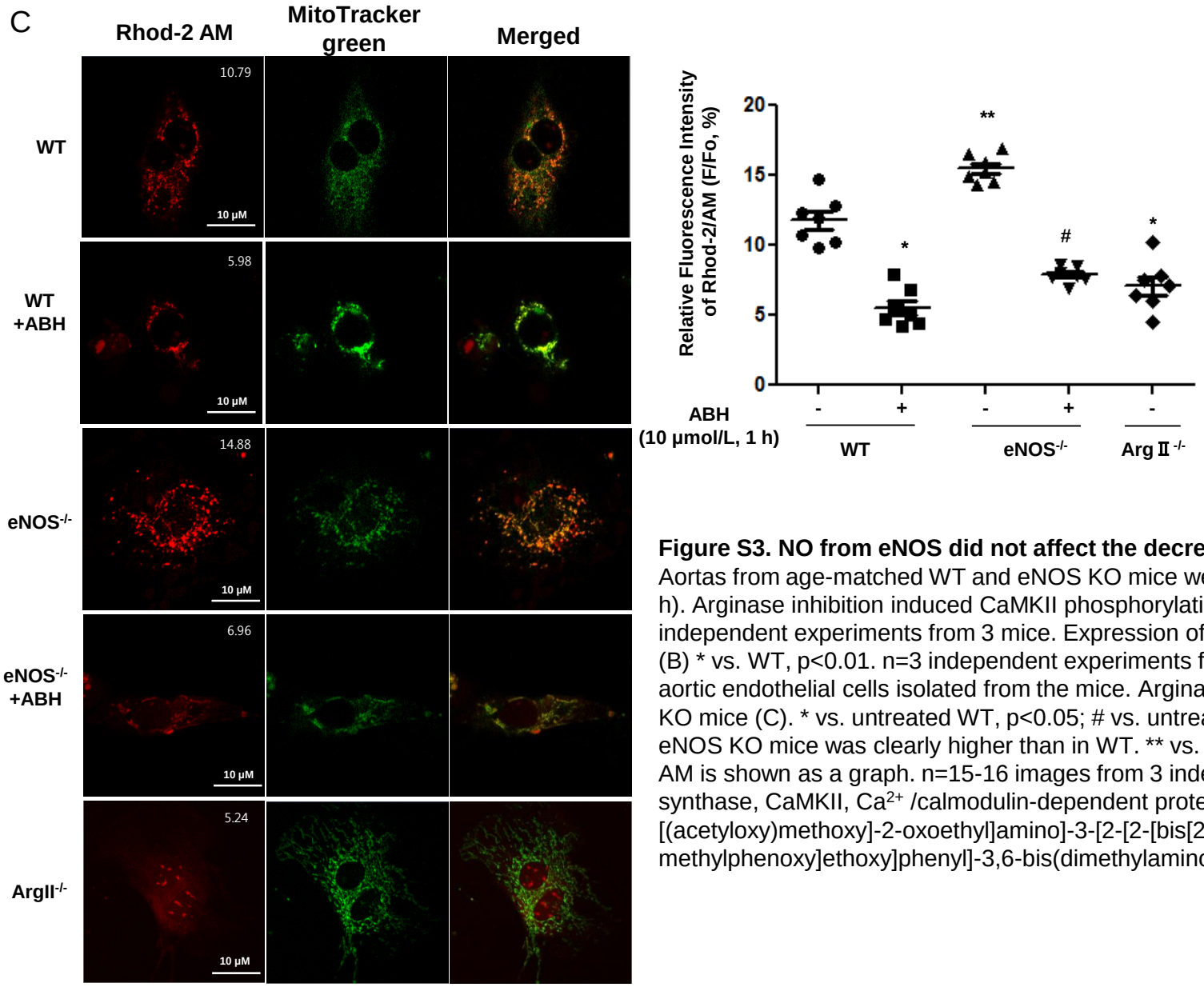

Figure S3. NO from eNOS did not affect the decreased $[Ca^{2+}]m$ caused by arginase II inhibition. Aortas from age-matched WT and eNOS KO mice were treated with the arginase inhibitor ABH (10 μmol/L, 1 h). Arginase inhibition induced CaMKII phosphorylation in these mice (A). * vs. untreated, $p<0.01$. n=3 independent experiments from 3 mice. Expression of (p32)m and arginase II was increased in eNOS KO mice (B) * vs. WT, $p<0.01$. n=3 independent experiments from 3 mice. $[Ca^{2+}]m$ was estimated with Rhod-2 AM in aortic endothelial cells isolated from the mice. Arginase inhibition decreased $[Ca^{2+}]m$ in both WT and eNOS KO mice (C). * vs. untreated WT, $p<0.05$; # vs. untreated eNOS KO, $p<0.01$. The basal level of $[Ca^{2+}]m$ in eNOS KO mice was clearly higher than in WT. ** vs. untreated WT, $p<0.05$. Fluorescence intensity of Rhod-2 AM is shown as a graph. n=15-16 images from 3 independent experiments. eNOS, endothelial nitric oxide synthase, CaMKII, Ca^{2+} /calmodulin-dependent protein kinase II, KO, knock-out, Rhod-2 AM, 9-[4-[Bis[2-[(acetyloxy)methoxy]-2-oxoethyl]amino]-3-[2-[2-[bis[2-[(acetyloxy)methoxy]-2-oxoethyl]amino]-5-methylphenoxy]ethoxy]phenyl]-3,6-bis(dimethylamino)xanthylium bromide, WT, wild type.

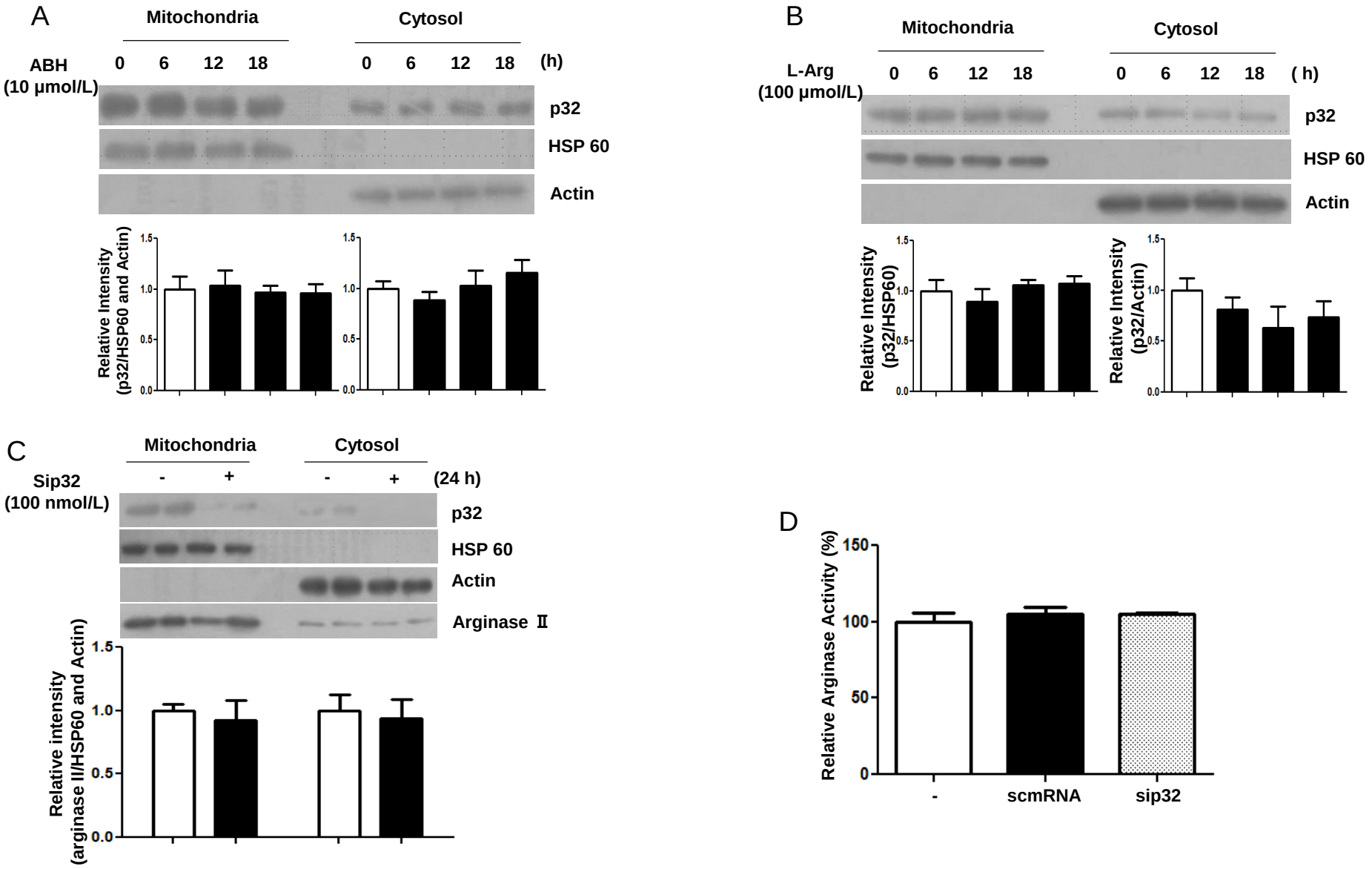

Figure S4. Arginase inhibition and L-Arg supplement had no effect on p32 protein level, and sip32 was not associated with arginase II expression and activity.

The arginase inhibitor ABH (A) and substrate L-Arg (B) were incubated with HUVECs for different time periods, and p32 protein expression was examined using western blot analysis after mitochondrial fractionation. HUVECs treated with sip32 were analyzed for arginase II expression (C) and arginase activity (D). n=3 independent experiments. L-Arg, L-arginine.

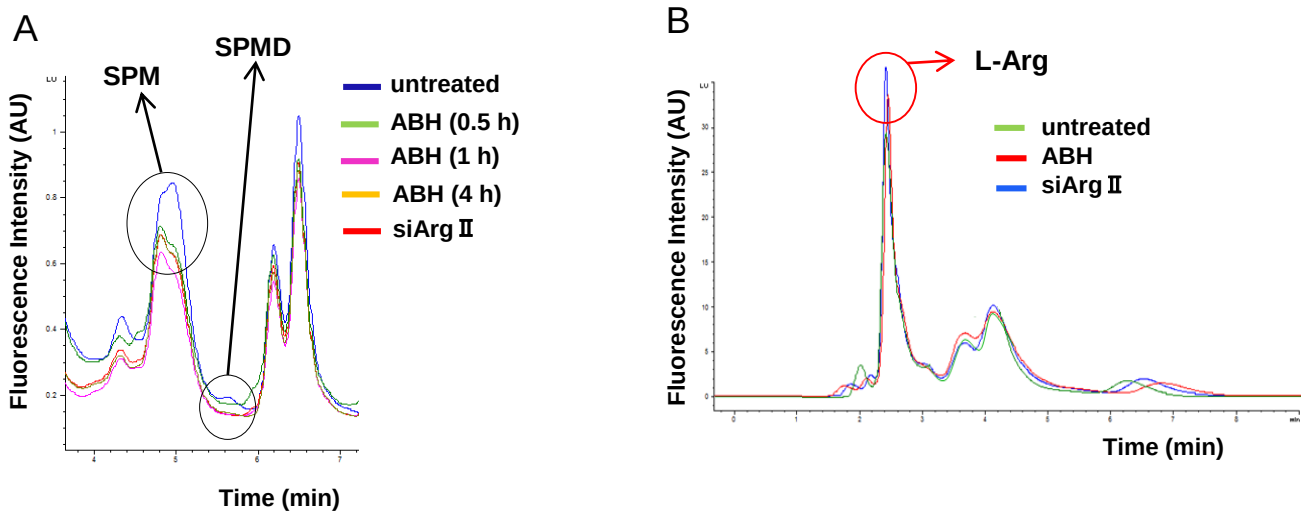

Figure S5. Arginase II inhibition decreased [SPM] and increased [L-Arg].
Arginase inhibition with ABH (10 μmol/L) and siArgII significantly decreased intracellular [SPM] (A). Conversely, L-Arg concentration was increased by arginase inhibition (B). Representative HPLC chromatogram of polyamine (A) and L-Arg analysis (B). n=3 independent experiments. SPM, spermine, L-Arg, L-arginine, HPLC, high Performance Liquid chromatography.

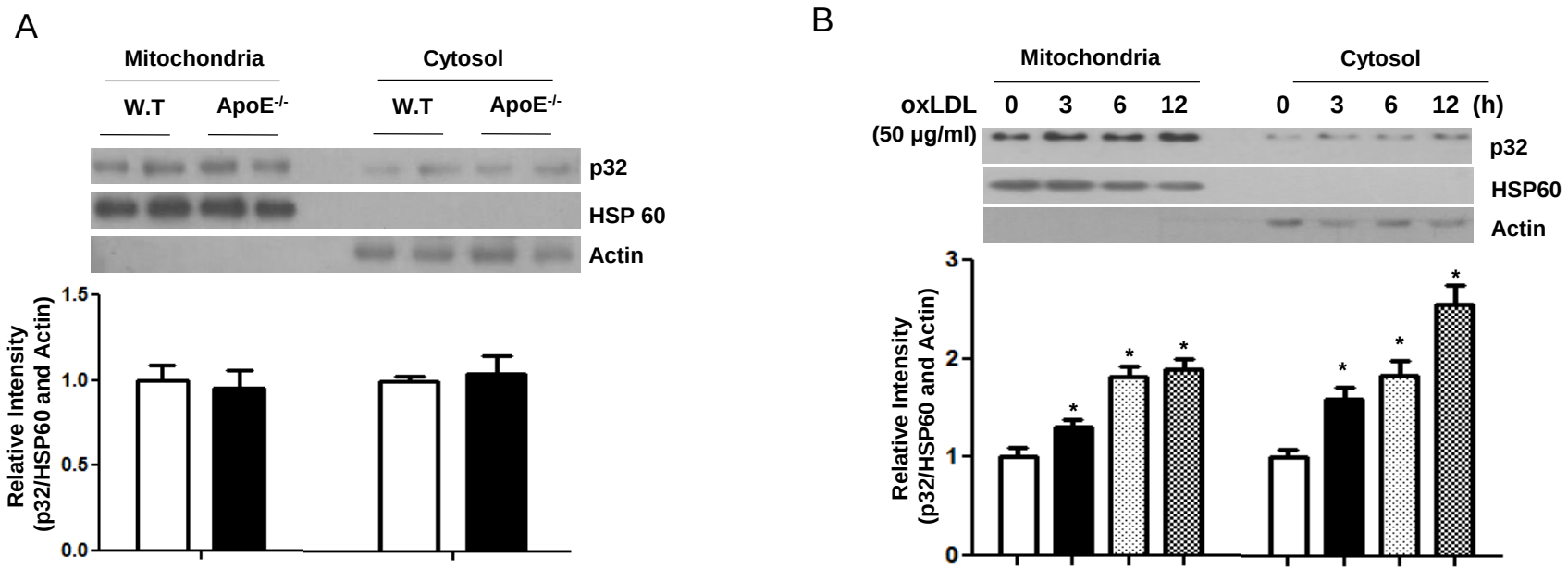

Figure S6. [p32]m was not changed in aortas of ApoE$^{-/-}$ mice fed an ND, and oxLDL stimulation induced p32 expression. p32 expression in aortic vessels from age-matched WT and ApoE$^{-/-}$ mice fed an ND was not different (A), but oxLDL stimulated p32 expression in aortas of WT mice (B). * vs. 0 h, $p<0.05$, n=3 independent experiments. ND, normal diet, OxLDL, oxidized low-density lipoprotein, WT, wild type, ApoE$^{-/-}$, ApoE-null mice.

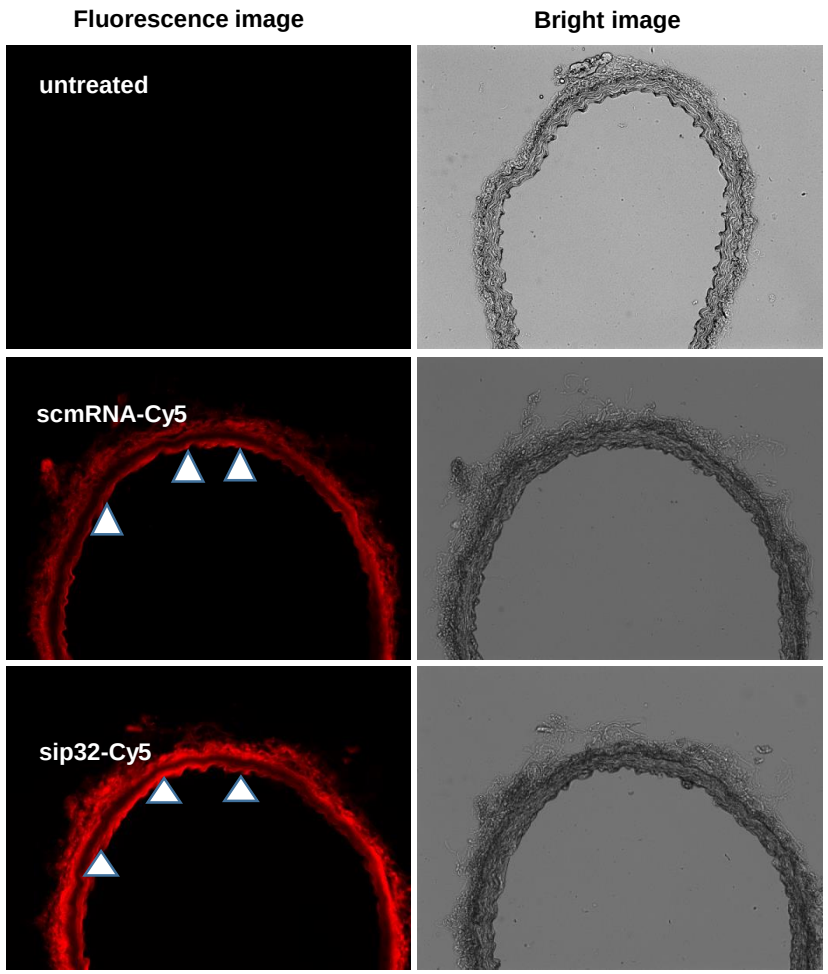

Figure S7. sip32 integrated into aortic vessel.
Cy-5-tagged siRNAs were administered by intravenous injection. Aortic vessels were cryosectioned and imaged to Cy-5 fluorescence. Arrows indicates endothelia. n= 3 mice. siRNA, small interfering RNA.

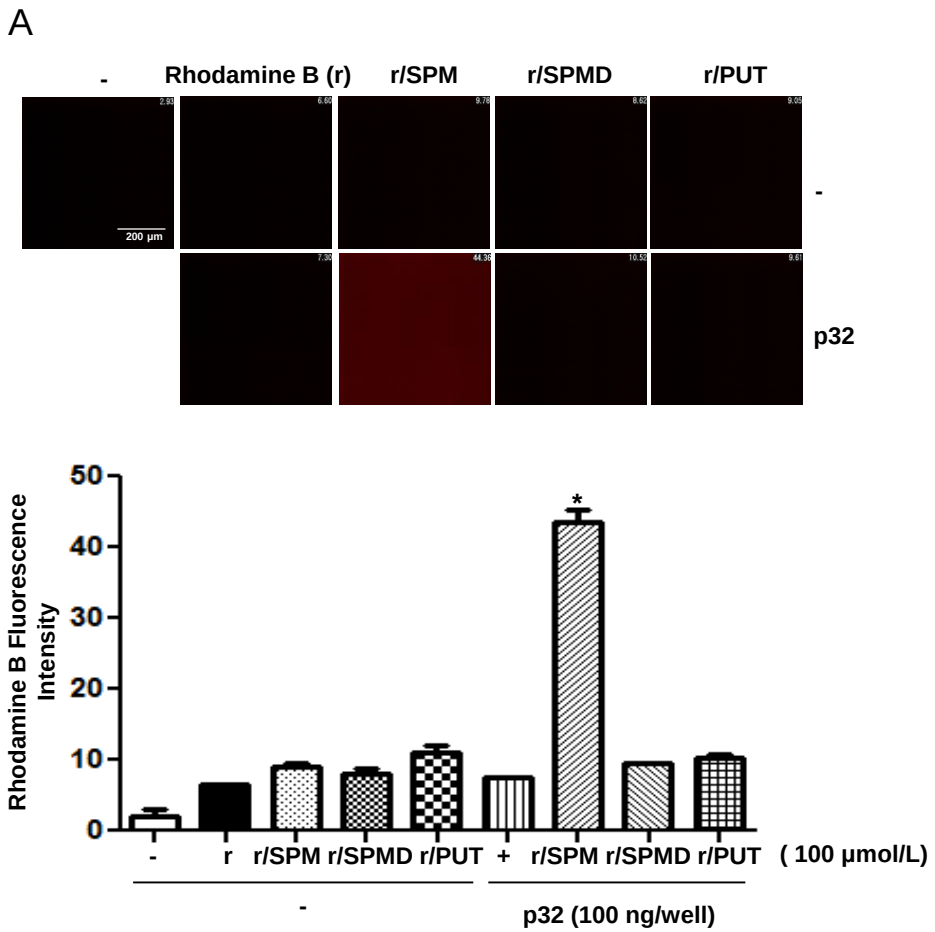

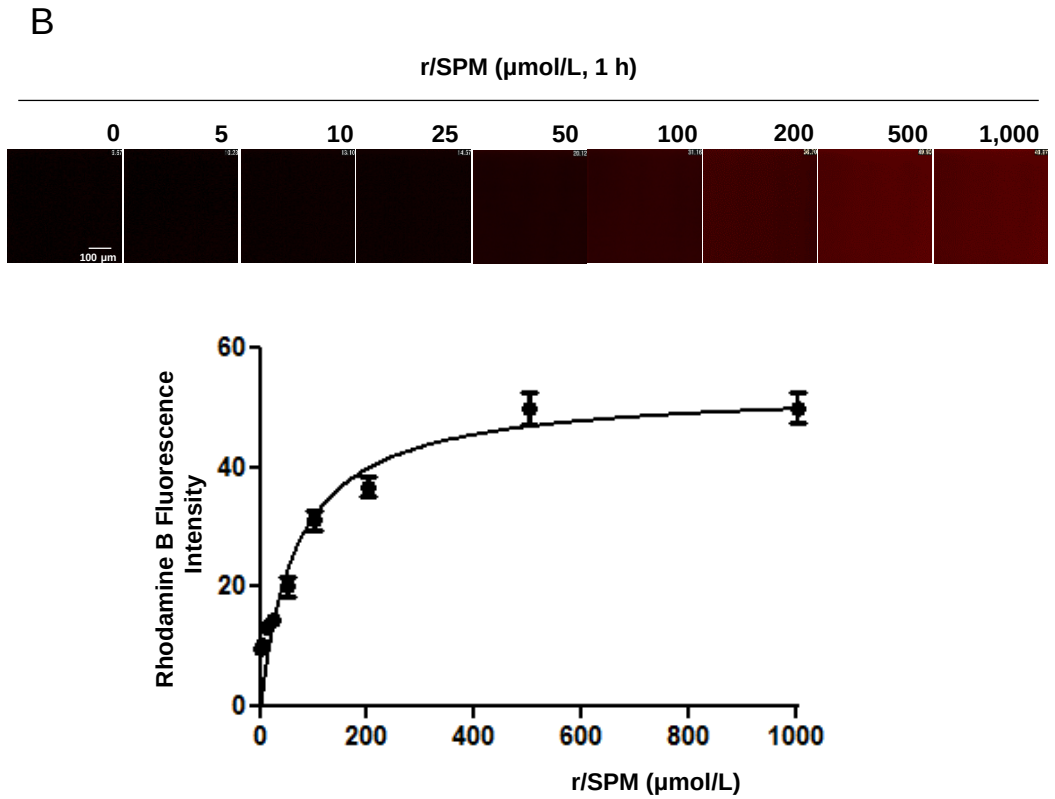

Figure S8. Interaction of p32 with SPM based on fluorescence immunoassay. Rhodamine B (r)-tagged polyamine was incubated with p32-coated and untreated wells. Rhodamine B-tagged SPM (r/SPM) bound to p32 (A). To examine the binding efficiency of SPM to p32, different concentrations of r/SPM were incubated with p32, and K_d value was 66.2 ± 4.8 μmol/L (B). n=3 independent experiments. SPM, spermine, r/SPM, rhodamine B-tagged spermine.

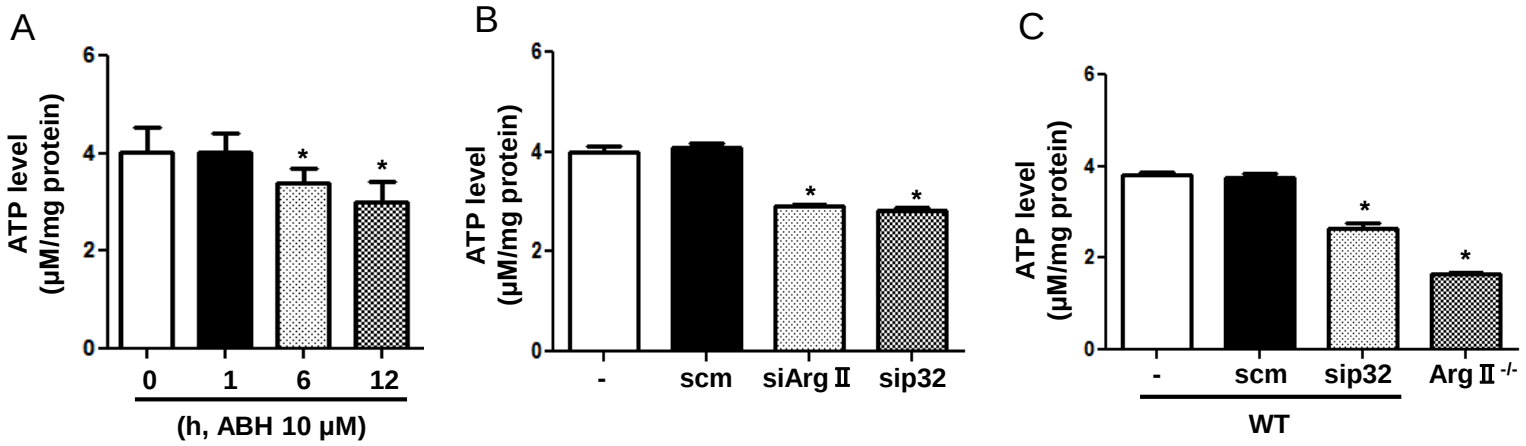

Figure S9. Arginase inhibition and sip32 treatment reduced intracellular ATP level. (A) Arginase inhibition with ABH during different time points decreased ATP content in HUVECs. (B) siArgII and sip32 decreased ATP level in HUVECs. (C) ATP level was decreased by incubating with sip32 in aortas of WT mice and lower ATP concentration was observed in aortas of ArgII$^{-/-}$ mice. * vs. untreated control, $p<0.05$, n=3 experiments. siArgII, siRNA against arginase II, ArgII$^{-/-}$, arginase II-null mice

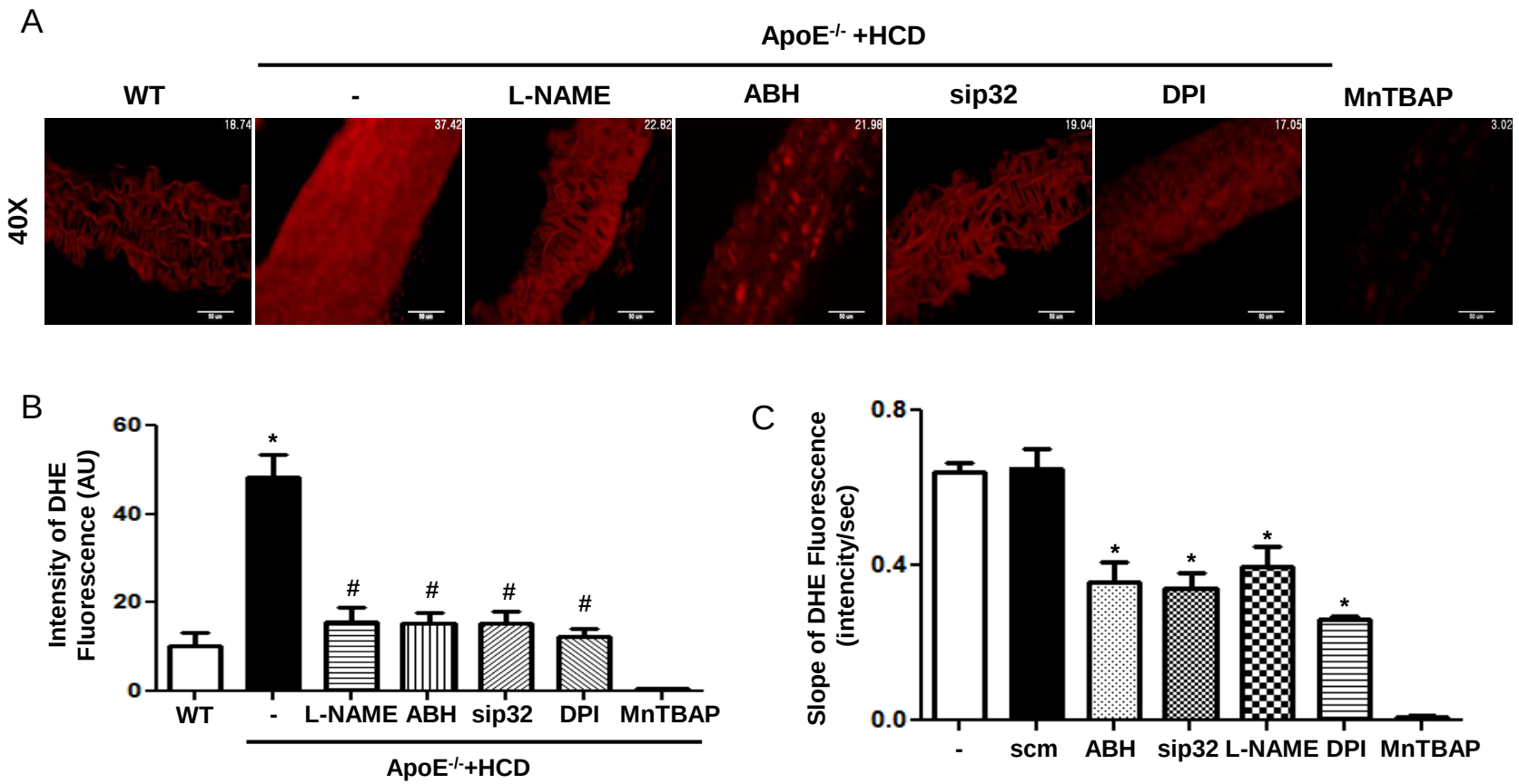

Figure S10. eNOS and NADPH oxidase were responsible for ROS production in aortas of ApoE$^{-/-}$ mice fed HCD. (A) Aortic vessels were sectioned and stained with DHE. (B) The fluorescence intensity of DHE were presented as bar graph. eNOS inhibitor (L-NAME), arginase inhibitor (ABH), sip32, and, NADPH oxidase inhibitor (diphenyleneiodonium, DPI) blocked ROS production. * vs. untreated control, $p<0.01$; # vs. ApoE$^{-/-}$+HCD, $p<0.01$, n=3 experiments. (C) Real-time measurement of ROS production using DHE in aortic endothelia showed the same results as presented at histological assay. * vs. untreated control, $p<0.01$, n=3 experiments. ROS, reactive oxygen species, DHE, dihydroethidium, HCD, high fat diet, L-NAME, N$^{\omega}$-Nitro-L-arginine methyl ester hydrochloride.